

Numerical twist-even $SU(1,1)$ -singlet solutions in open string field theory around the identity-based solution

Isao KISHIMOTO^{1*} and Tomohiko TAKAHASHI^{2†}

¹*Center for Liberal Arts and Sciences, Sanyo-Onoda City University,
Daigakudori 1-1-1, Sanyo-Onoda Yamaguchi 756-0884, Japan*

²*Department of Physics, Nara Women's University,
Nara 630-8506, Japan*

Abstract

Using the level truncation method, we construct numerical solutions, which are twist even and $SU(1,1)$ singlet, in the theory around the Takahashi-Tanimoto identity-based solution (TT solution) with a real parameter a in the framework of bosonic open string field theory. We find solutions corresponding to “double brane” and “ghost brane” solutions which were constructed by Kudrna and Schnabl in the conventional theory around the perturbative vacuum. Our solutions show somewhat similar a -dependence to tachyon vacuum and single brane solutions, which we found in the earlier works. In this sense, we might be able to expect that they are consistent with the conventional interpretation of a -dependence of the TT solution. We observe that numerical complex solutions at low levels become real ones at higher levels for some region of the parameter a . However, these real solutions do not so improve interpretation for double brane.

*ikishimo@rs.socu.ac.jp

†tomo@asuka.phys.nara-wu.ac.jp

Contents

1	Introduction	2
2	Procedure for constructing numerical solutions	3
3	“Double brane” solution	6
3.1	Energy	6
3.2	Gauge invariant observable	8
3.3	$ \Delta_S $ and reality	10
4	“Ghost brane” solution	12
4.1	Energy	12
4.2	Gauge invariant observable	14
4.3	$ \Delta_S $ and reality	16
5	Concluding remarks	16
A	Some numerical data for solutions	18
A.1	Numerical data for solutions at $a = -1/2$	18
A.2	Coefficients of lowest level states for the solutions	18
A.3	Evaluation of quadratic identities	18

1 Introduction

In bosonic open string field theory, there is a well-known numerical solution: the tachyon vacuum solution in Siegel gauge. It was found by Sen and Zwiebach [1] using the level truncation method and then higher level calculations were performed for the solution [2, 3, 4, 5]. It is known that efficient and consistent truncation for it can be obtained by restricting the space of string fields to that spanned by twist even and $SU(1,1)$ singlet states. With the same restriction, but relaxing the reality condition, Kudrna and Schnabl constructed two interesting solutions [5], which might be interpreted as double brane and ghost brane, respectively.

Numerical solutions mentioned above can be constructed using Newton’s method by choosing appropriate initial configurations so that iterative calculations converge. The tachyon vacuum solution can be uniquely obtained from a real solution at the level 0, namely, the lowest truncation level. The “double brane” and “ghost brane” solutions can be obtained from one of complex solutions, which do not satisfy the reality condition for string fields, at the truncation level 2 and 4, respectively.

On the other hand, the Takahashi-Tanimoto (TT) solution [6] is based on the identity string field and therefore direct evaluation of its energy was difficult. Alternatively, in the theory around the TT solution, the BRST cohomology was studied [7] and numerical solutions in Siegel gauge were investigated [8, 9, 10]. The TT solution has a real parameter a such as $a \geq -1/2$ and it is expected that it represents the tachyon vacuum at $a = -1/2$ and is pure gauge for $a > -1/2$. It was supported by analysis of cohomology in [7] and evaluation of energy of the tachyon vacuum solution in Siegel gauge [8] in the theory around the TT solution (Ψ_a^{TT}). Furthermore, numerical solution for unstable vacuum, which corresponds to the perturbative vacuum or single brane, was found in [9] in the theory around Ψ_a^{TT} for $a \simeq -1/2$.¹

In this paper, motivated by “double brane” and “ghost brane” solutions found in [5], we construct numerical twist-even $SU(1,1)$ -singlet solutions, which correspond to them, in the theory around Ψ_a^{TT} for $a \geq -1/2$. They show somewhat similar a -dependence to the tachyon vacuum and single brane solutions. Namely, with increasing level, energy of them seems to approach a constant E for $a > -1/2$ and another value E' for $a \simeq -1/2$ ($E' > E$). However, the numerical behaviors of them are not so clear. Actually, the values of energy are complex in general because these numerical solutions are obtained from one of complex solutions in the truncation level 2 and 4. Roughly, the imaginary part of the energy for them seems to approach zero with increasing level. Particularly, we find that these solutions in the theory around Ψ_a^{TT} for some region of a satisfy the reality condition at higher levels although they start from complex solutions at the level 2 or 4.

Here, we have performed numerical calculations up to the truncation level 22, and the values of the energy and the gauge invariant observable² for “double brane” and “ghost brane” solutions might (not) represent the number of branes literally. Further investigation is necessary for a definite interpretation.

This paper is organized as follows. In §2, we will explain our strategy of numerical calculations and conventions briefly. In §3 and §4, we will show our numerical results: plots of energy, gauge invariant observables and so on, for “double brane” solution and “ghost brane” solution, respectively. In §5,

¹The energy of Ψ_a^{TT} is calculated analytically in [11, 12] and it is confirmed that the TT solution is the tachyon vacuum at $a = -1/2$ and is pure gauge for $a > -1/2$.

²It is also called gauge invariant overlap or Ellwood invariant in the literatures.

we will give some remarks on our calculations. Moreover, in appendix A, we will give some explicit numerical data for the solutions at $a = -1/2$ including evaluations of quadratic identities.

2 Procedure for constructing numerical solutions

In this section, we briefly explain procedure to construct numerical solutions and we define quantities to evaluate for the solutions. Further technical details can be found in [5].

The TT solution Ψ_a^{TT} [6], with a real parameter a such as $a \geq -1/2$, is one of identity-based solutions to the equation of motion $Q_B \Psi + \Psi * \Psi = 0$ in open string field theory, whose action is $S[\Psi] = -\frac{1}{g^2} \left(\frac{1}{2} \langle \Psi, Q_B \Psi \rangle + \frac{1}{3} \langle \Psi, \Psi * \Psi \rangle \right)$, where Q_B is the conventional BRST operator. Around the TT solution Ψ_a^{TT} , we define the action $S_a[\Phi]$ as³

$$S_a[\Phi] = S[\Psi_a^{\text{TT}} + \Phi] - S[\Psi_a^{\text{TT}}] = -\frac{1}{g^2} \left(\frac{1}{2} \langle \Phi, Q' \Phi \rangle + \frac{1}{3} \langle \Phi, \Phi * \Phi \rangle \right), \quad (2.1)$$

$$Q' = (1+a)Q_B + \frac{a}{2}(Q_2 + Q_{-2}) + 4aZ(a)c_0 - 2aZ(a)^2(c_2 + c_{-2}) \\ + 2a(1-Z(a)^2) \sum_{n=2}^{\infty} (-Z(a))^{n-1} (c_{2n} + c_{-2n}), \quad (2.2)$$

$$Z(a) = \frac{1+a-\sqrt{1+2a}}{a}, \quad (2.3)$$

where Q_n is a mode of the BRST current. In the case $a = 0$, Ψ_a^{TT} becomes zero, namely $\Psi_{a=0}^{\text{TT}} = 0$, and hence $Q'|_{a=0} = Q_B$. The equation of motion of (2.1) is

$$Q' \Phi + \Phi * \Phi = 0 \quad (2.4)$$

and it is projected to

$$L(a)\Phi + b_0(\Phi * \Phi) = 0, \quad (2.5)$$

$$L(a) = (1+a)(L_0^{\text{mat}} + L_0^{\text{gh}} - 1) + \frac{a}{2}(L_2^{\text{mat}} + L_2^{\text{gh}} + L_{-2}^{\text{mat}} + L_{-2}^{\text{gh}}) + 4(1+a-\sqrt{1+2a}), \quad (2.6)$$

using the Siegel gauge condition: $b_0 \Phi = 0$. Here, L_n^{mat} is the Virasoro generator in the matter sector with the central charge 26 and L_n^{gh} is a twisted Virasoro generator in the ghost sector with the central charge -2 , which is given by

$$L_n^{\text{gh}} = \sum_{m=-\infty}^{\infty} (n-m) : b_m c_{n-m} : \quad (2.7)$$

in terms of the bc -ghost modes. In order to solve a nonlinear equation (2.5), we use Newton's method as follows. Firstly, we take an initial string field $\Phi^{(0)}$, then we solve a linearized equation:

$$L(a)\Phi^{(n+1)} + b_0(\Phi^{(n)} * \Phi^{(n+1)}) + b_0(\Phi^{(n+1)} * \Phi^{(n)}) = b_0(\Phi^{(n)} * \Phi^{(n)}) \quad (2.8)$$

³We take the case of $l = 1$ for the TT solution, where an integer l was introduced in [7]. Similar computations can be performed for $l = 2, 3, 4, \dots$, but $l = 1$ is the most fundamental in the context of the level truncation in the sense that mixing of the levels in the kinetic term is minimum in Siegel gauge.

for $n = 0, 1, 2, \dots$, iteratively. If $\Phi^{(n)}$ converges to a string field with $n \rightarrow \infty$, $\Phi^{(\infty)}$ is a solution to (2.5). Actually, we stop the calculation when $\|\Phi^{(n+1)} - \Phi^{(n)}\|/\|\Phi^{(n)}\| < \varepsilon$ for a sufficiently small positive constant ε , where $\|\cdot\|$ is a norm and we regard $\Phi^{(n+1)}$ as an approximate solution.

We adopt the level truncation method to take a finite number of component fields from a string field Φ for numerical calculation. As a consistent level L truncation, where L is the eigenvalue of $L_0^{\text{mat}} + L_0^{\text{gh}}$, we expand a string field of the ghost number one with a basis which consists of twist even and $\text{SU}(1,1)$ singlet states of the form:

$$L_{-n_m}^{\text{mat}} \cdots L_{-n_1}^{\text{mat}} L_{-l_g}^{\text{gh}} \cdots L_{-l_1}^{\text{gh}} c_1 |0\rangle, \quad (2.9)$$

$$n_m \geq \cdots \geq n_1 \geq 2, \quad l_g \geq \cdots \geq l_1 \geq 2, \quad \sum_{k=1}^m n_k + \sum_{k=1}^g l_k = \ell, \quad (\ell = 0, 2, 4, \dots, L). \quad (2.10)$$

The truncation level L is an even integer from the twist even condition and $|0\rangle$ is the conformal vacuum. We denote a state of the above form as ψ_i and we expand Φ as

$$\Phi = \sum_{i=1}^{N_L} t_i \psi_i, \quad (2.11)$$

with coefficients t_i , where N_L is the dimension of the truncated state space up to level L , namely, $N_L = 1, 3, 8, 21, 51, 117, \dots$ for $L = 0, 2, 4, 6, 8, 10, \dots$, respectively. We take t_i as a complex constant in general although it should be real from the reality condition of string fields. It is necessary to construct “double brane” and “ghost brane” solutions as we will see later.

With the above level truncation of string fields, we take a BPZ inner product of $c_0 \psi_i$ and (2.8) and we obtain simultaneous equations:

$$\sum_{j=1}^{N_L} \left((L(a))_{ij} + 2 \sum_{k=1}^{N_L} V_{ijk} t_k^{(n)} \right) t_j^{(n+1)} = \sum_{j,k=1}^{N_L} V_{ijk} t_k^{(n)} t_j^{(n)}, \quad (2.12)$$

where

$$(L(a))_{ij} = \langle \psi_i, c_0 L(a) \psi_j \rangle, \quad V_{ijk} = \langle \psi_i, \psi_j * \psi_k \rangle, \quad (2.13)$$

and use has been made of $V_{ijk} = V_{ikj}$ thanks to the twist even condition. With appropriate initial values $\{t_i^{(0)}\}_{i=1,2,\dots,N_L}$ ($t_i^{(0)} \in \mathbb{C}$), we solve (2.12) iteratively for $n = 0, 1, 2, \dots$. We stop the calculation if $\|\mathbf{t}^{(n+1)} - \mathbf{t}^{(n)}\|/\|\mathbf{t}^{(n)}\| < \varepsilon$ with the Euclidean norm for a sufficiently small positive ε and we regard

$$\Phi_a = \sum_{i=1}^{N_L} \tilde{t}_i \psi_i. \quad (2.14)$$

($\tilde{t}_i = t_i^{(n+1)}$) as a numerical solution to (2.5).⁴

⁴In our actual calculation in §3 and §4, we took $\varepsilon = 5 \times 10^{-14}$ in our C++ code with the long double format. If $\|\mathbf{t}^{(n+1)} - \mathbf{t}^{(n)}\|/\|\mathbf{t}^{(n)}\| \geq \varepsilon$ for $n + 1 = 15$, we regarded it as not converging.

For a numerical solution Φ_a , we compute the energy $E[\Phi_a]$, which is given by the action (2.1) as

$$E[\Phi_a] = 1 - 2\pi^2 g^2 S_a[\Phi_a] = 1 + \frac{\pi^2}{3} \sum_{i,j=1}^{N_L} (L(a))_{ij} \tilde{t}_i \tilde{t}_j, \quad (2.15)$$

where we have used the equation of motion for $\tilde{\mathbf{t}}$:

$$\sum_{j=1}^{N_L} (L(a))_{ij} \tilde{t}_j + \sum_{j,k=1}^{N_L} V_{ijk} \tilde{t}_k \tilde{t}_j = 0. \quad (2.16)$$

$E[\Phi_a]$ (2.15) is normalized in the same way as [5]. In the case $a = 0$, or in the theory around the perturbative vacuum, $E[0]|_{a=0} = 1$ for the single brane solution 0, which is the perturbative vacuum, and $E[\Psi^T]|_{a=0} = 0$ for the tachyon vacuum solution Ψ^T .

We evaluate the gauge invariant observable $E_0[\Phi_a]$ for Φ_a :

$$E_0[\Phi_a] = 1 - 2\pi \langle I|V|\Phi_a \rangle \quad (2.17)$$

where V is given by $c(i)c(-i)\mathcal{V}(i, -i)$ and $\mathcal{V}(z, \bar{z})$ is matter primary with conformal weight $(1, 1)$ and is normalized as

$$\langle I|V|c_1|0 \rangle = \frac{1}{4}. \quad (2.18)$$

We note that (2.17) satisfies $E_0[\Psi_{\text{Sch}}] = 0$ [13, 14] for Schnabl's analytic solution for tachyon condensation Ψ_{Sch} [15].

For the tachyon vacuum solution Φ_a^T and the perturbative vacuum (or single brane) solution Φ_a^S , in the theory around the TT solution Ψ_a^{TT} ($a \geq -1/2$), it has been shown that E (2.15) and E_0 (2.17) behave as

$$E[\Phi_a^T] \rightarrow \begin{cases} 0 & (a > -1/2) \\ 1 & (a = -1/2) \end{cases}, \quad E_0[\Phi_a^T] \rightarrow \begin{cases} 0 & (a > -1/2) \\ 1 & (a = -1/2) \end{cases}, \quad (2.19)$$

$$E[\Phi_a^S] \rightarrow \begin{cases} 1 & (a > -1/2) \\ 2 & (a = -1/2) \end{cases}, \quad E_0[\Phi_a^S] \rightarrow \begin{cases} 1 & (a > -1/2) \\ 2 & (a = -1/2) \end{cases}, \quad (2.20)$$

numerically in the large truncation level limit $L \rightarrow \infty$, where $\Phi_{a=-1/2}^T \rightarrow 0$ and $\Phi_{a>-1/2}^S \rightarrow 0$ [9].

As a consistency of the equation of motion (2.4) for numerical solutions to (2.5), we evaluate

$$|\Delta_S[\Phi_a]| = |\langle 0|c_{-1}b_2c_0|Q'\Phi_a + \Phi_a * \Phi_a \rangle| \quad (2.21)$$

after [5]. It is the lowest level verification of BRST invariance for Siegel gauge solutions in the context of [16]. Furthermore, we evaluate

$$\text{Im/Re}[\Phi_a] = \frac{\|\text{Im } \tilde{\mathbf{t}}\|}{\|\text{Re } \tilde{\mathbf{t}}\|} \quad (2.22)$$

for reality of numerical solutions, which is given by the ratio of the Euclidean norm of imaginary and real part of $\tilde{\mathbf{t}}$.

3 “Double brane” solution

In the theory around the perturbative vacuum, which is the case $a = 0$ in (2.1), a “double brane” solution $\Phi_{a=0}^D$ is obtained from one of complex solutions at the truncation level 2. Taking a solution $\Phi_{a=0}^D$ at level L as an initial string field, we can obtain $\Phi_{a=0}^D$ at level $L + 2$ by Newton’s method as explained in §2. Such a solution $\Phi_{a=0}^D$ coincides with the “double brane” solution in [5].

In the case $a \neq 0$, we adopt a strategy to construct solutions Φ_a^D corresponding to “double brane” as follows:

1. At level 2, we construct a solution $\Phi_{a \mp \epsilon}^D$ using Newton’s method with an initial string field Φ_a^D . We repeat this calculation with $\epsilon = 0.001$ up to $\Phi_{a \mp 1/2}^D$ from the starting point $\Phi_{a=0}^D$.
2. At level $L + 2$, we construct a solution Φ_a^D using Newton’s method with an initial string field Φ_a^D at level L . We repeat this calculation up to level 22.

Namely, for a fixed value of a , which is one of $a = -0.5, -0.499, -0.498, \dots, 0.499, 0.5$, we constructed higher level solutions Φ_a^D from level 2 up to 22, level by level.

Then, we have obtained numerical solutions Φ_a^D , except for $\Phi_{a=-0.468}^D$ at levels 20 and 22. In the case $a = -0.468$, Newton’s method for getting a solution at level 20 did not converge.

3.1 Energy

Figs. 1, 2, and 3 show plots of the energy E (2.15) for the “double brane” solution Φ_a^D at the truncation level L . We joined adjacent calculated data points with line segments for each level.⁵ In Fig. 1, the dotted and dashed lines are extrapolations to $L = 4k + 2$ ($k \rightarrow \infty$) and $L = 4k$ ($k \rightarrow \infty$), respectively. We have used a polynomial of $1/L$ as a fitting function for each value of the parameter a . We have chosen its degree as the number of data minus one.⁶ As might be expected from Fig. 2, extrapolations by a polynomial fit worked well by dividing data in two groups: $L \equiv 2 \pmod{4}$ and $L \equiv 0 \pmod{4}$.

As in Fig. 1, the real part of energy $\text{Re} E[\Phi_a^D]$ approaches a constant, which is greater than one, for $a > -1/2$ with increasing level and there is a maximum at $a = a_M \sim -1/2$ for each L . As in Fig 2, the value of a_M approaches $-1/2$ with increasing level, where the maximum value is greater than two. The extrapolation values of $\text{Re} E[\Phi_a^D]$ in Fig. 1 are close to 1.5 for $a > -1/2$.

As in Fig. 3, the imaginary part of energy $\text{Im} E[\Phi_a^D]$ approaches zero for $a > -1/2$ with increasing level and there is a minimum at $a = a_m \sim -1/2$ for each L . The extrapolation values of $\text{Im} E[\Phi_a^D]$ in Fig. 3 are close to zero for $a > -1/2$. We observed that a_m approaches $-1/2$ and the minimum value approaches zero with increasing level although extrapolation values are unstable near $a = -1/2$.

From the above observation and analogy with tachyon vacuum and single brane solutions in (2.19) and (2.20), we could expect that the energy (2.15) for the “double brane” solution Φ_a^D behaves as

$$E[\Phi_a^D] \rightarrow \begin{cases} E_2 & (a > -1/2) \\ E'_2 & (a = -1/2) \end{cases} \quad (L \rightarrow \infty), \quad (3.1)$$

⁵Plots of other figures in this paper are in the same manner.

⁶Extrapolations in other figures in this paper have been obtained in the same manner.

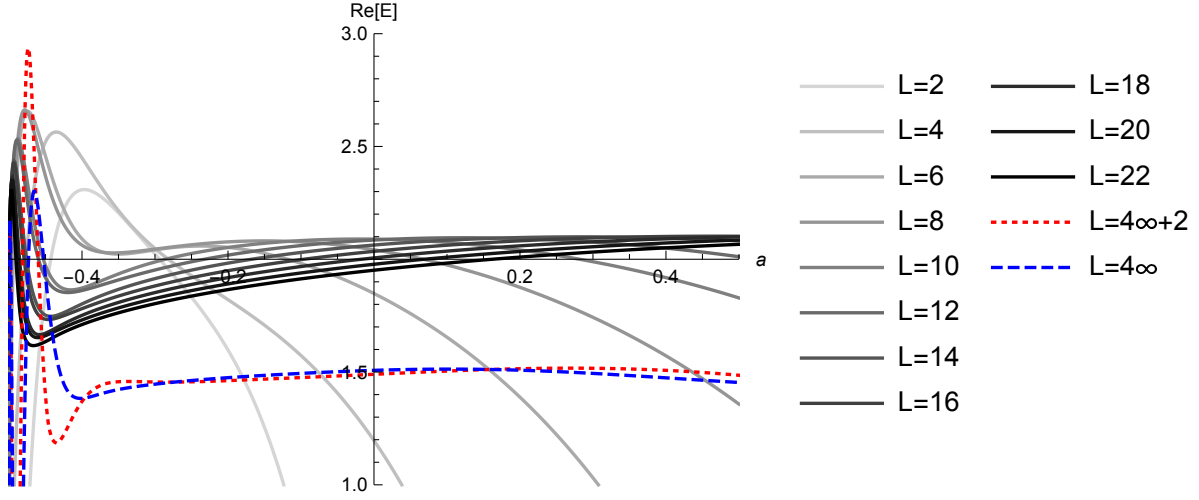


Figure 1: Plots of the real part of the energy E (2.15) for the “double brane” solution Φ_a^D at the truncation level L . The dotted and dashed lines are extrapolations to $L = 4k + 2$ ($k \rightarrow \infty$) and $L = 4k$ ($k \rightarrow \infty$), respectively. The horizontal axis denotes the value of the parameter a at $\text{Re } E = 2$.

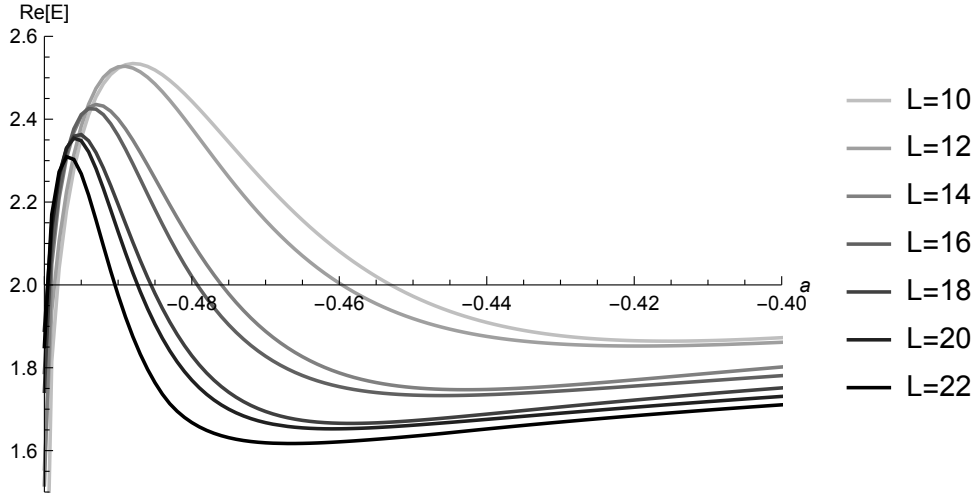


Figure 2: Plots of the real part of the energy E (2.15) for the “double brane” solution Φ_a^D such as $a \gtrsim -1/2$ at the truncation level $L = 10, 12, \dots, 22$. The horizontal axis denotes the value of the parameter a at $\text{Re } E = 2$. The vertical axis stands at $a = -1/2$.

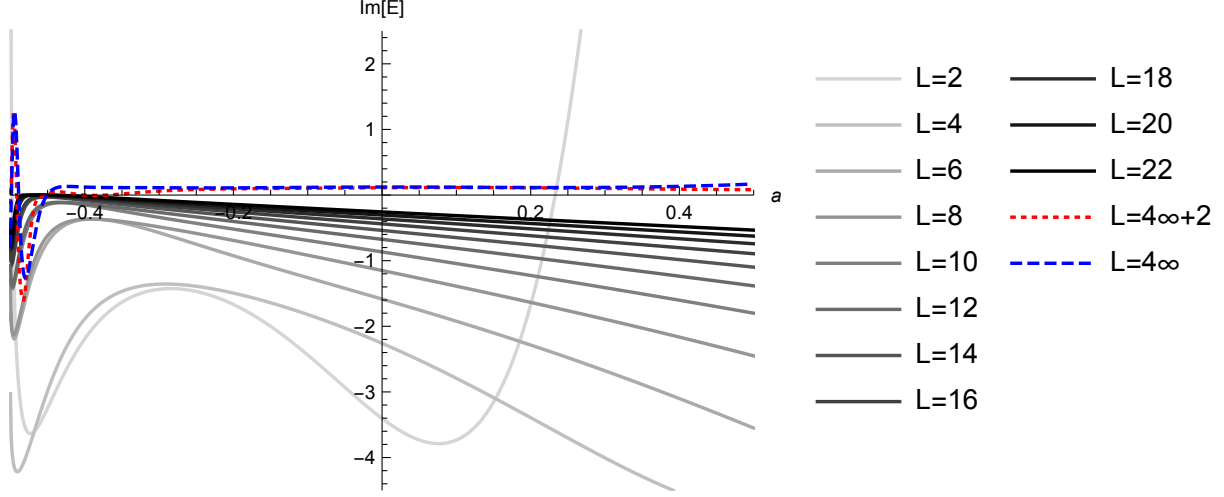


Figure 3: Plots of the imaginary part of the energy E (2.15) for the “double brane” solution Φ_a^D at the truncation level L . The dotted and dashed lines are extrapolations to $L = 4k + 2$ ($k \rightarrow \infty$) and $L = 4k$ ($k \rightarrow \infty$), respectively. The horizontal axis denotes the value of the parameter a .

where E_2 and E'_2 seem to be real constants and satisfy $1 < E_2 < E'_2$. If $E_2 = 2$ and $E'_2 = 3$, Φ_a^D could be interpreted as double brane solution for $a \geq -1/2$ literally. However, it seems that $E_2 \sim 1.5$ and $2 < E'_2 < 3$ from Figs. 1 and 2. If $E'_2 - E_2 = 1$, the solution Φ_a^D for $a \geq -1/2$ is consistent with the interpretation that the TT solution Ψ_a^{TT} represents the tachyon vacuum at $a = -1/2$ and pure gauge solution for $a > -1/2$, which implies $S[\Psi_{a=-1/2}^{TT}] = 1/(2\pi^2 g^2)$ and $S[\Psi_{a>-1/2}^{TT}] = 0$.

3.2 Gauge invariant observable

Figs. 4, 5, and 6 show plots of the gauge invariant observable E_0 (2.17) for the “double brane” solution Φ_a^D at the truncation level L .

As in Fig. 4, the real part $\text{Re } E_0[\Phi_a^D]$ approaches a constant, which is greater than one, for $a > -1/2$ with increasing level. As in Fig. 5 (and Table 1 in appendix A), $\text{Re } E_0[\Phi_a^D] > 2$ for $a \rightarrow -1/2 + 0$. The extrapolation values of $\text{Re } E_0[\Phi_a^D]$ in Fig. 4 are close to 1.2 for $a > -1/2$ although they become unstable near $a = -1/2$. This instability or error should be caused by irregular behavior around $a = -0.465$ at $L = 20, 22$ in Fig. 5.

As in Fig. 6, the imaginary part $\text{Im } E_0[\Phi_a^D]$ approaches zero for $a > -1/2$ with increasing level. The extrapolation values are around zero for $a > -1/2$ although they are unstable near $a = -1/2$. Actually, we have found that $\text{Im } E_0[\Phi_a^D] = 0$ around $a = -0.465$ for $L = 20, 22$.

From the above, in a similar way to (3.1), we could expect that the gauge invariant observable (2.17) behaves as

$$E_0[\Phi_a^D] \rightarrow \begin{cases} \tilde{E}_2 & (a > -1/2) \\ \tilde{E}'_2 & (a = -1/2) \end{cases} \quad (L \rightarrow \infty), \quad (3.2)$$

where \tilde{E}_2 and \tilde{E}'_2 seem to be real constants and satisfy $1 < \tilde{E}_2 < \tilde{E}'_2$. If $\tilde{E}_2 = 2$ and $\tilde{E}'_2 = 3$, Φ_a^D could be interpreted as double brane solution for $a \geq -1/2$ because the value of (2.17) corresponds to the

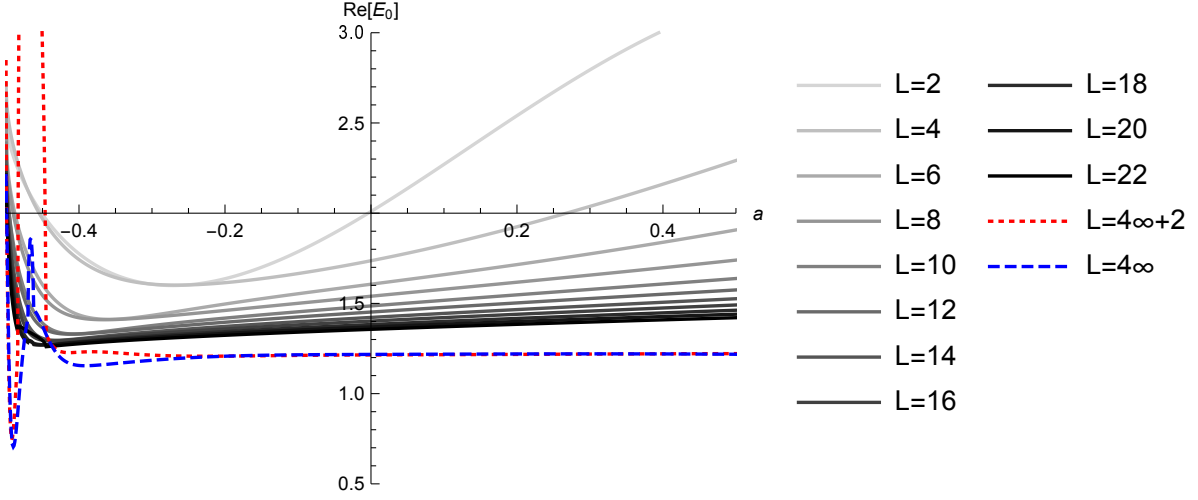


Figure 4: Plots of the real part of the gauge invariant observable E_0 (2.17) for the “double brane” solution Φ_a^D at the truncation level L . The dotted and dashed lines are extrapolations to $L = 4k + 2$ ($k \rightarrow \infty$) and $L = 4k$ ($k \rightarrow \infty$), respectively. The horizontal axis denotes the value of the parameter a at $\text{Re } E_0 = 2$.

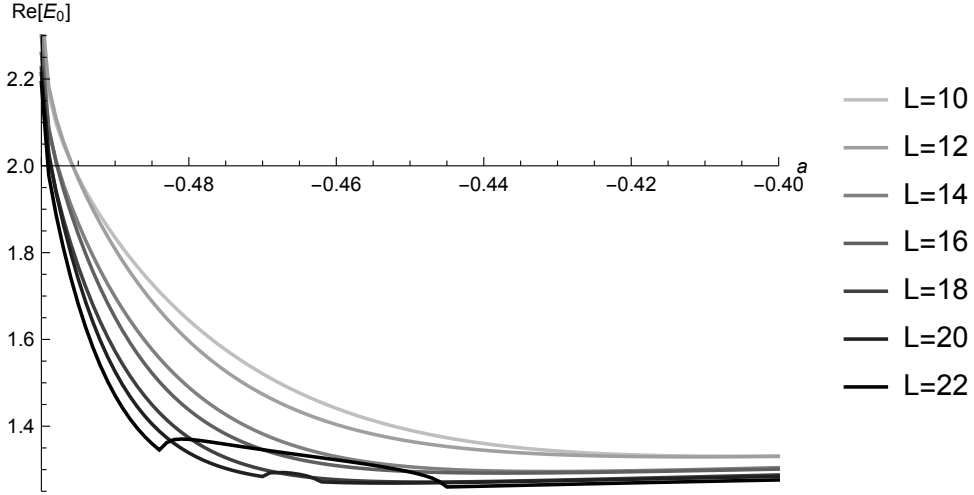


Figure 5: Plots of the real part of the gauge invariant observable E_0 (2.17) for the “double brane” solution Φ_a^D such as $a \gtrsim -1/2$ at the truncation level $L = 10, 12, \dots, 22$. The horizontal axis denotes the value of the parameter a at $\text{Re } E_0 = 2$. The vertical axis stands at $a = -1/2$.

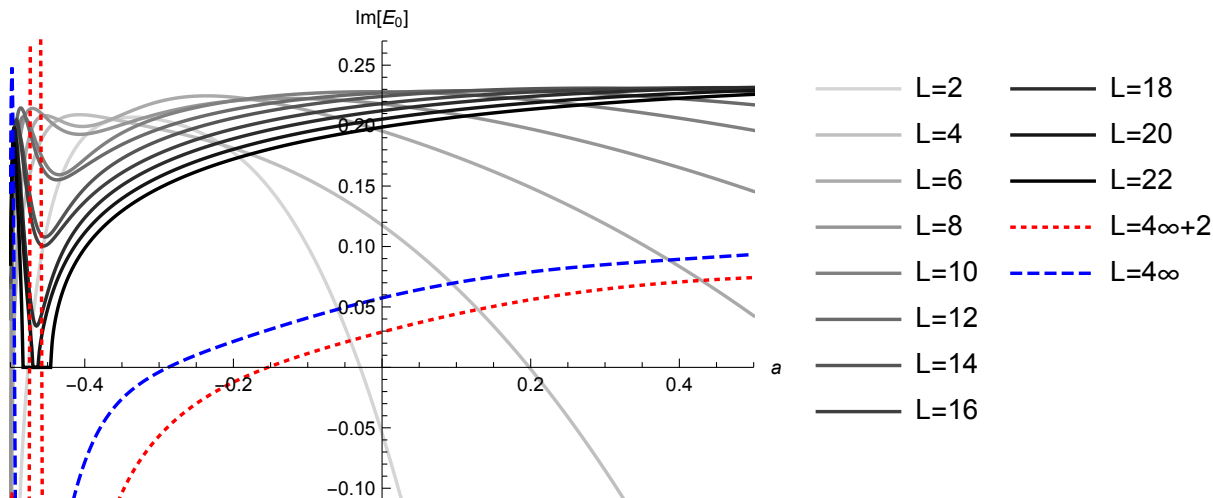


Figure 6: Plots of the imaginary part of the gauge invariant observable E_0 (2.17) for the “double brane” solution Φ_a^D at the truncation level L . The dotted and dashed lines are extrapolations to $L = 4k + 2$ ($k \rightarrow \infty$) and $L = 4k$ ($k \rightarrow \infty$), respectively. The horizontal axis denotes the value of the parameter a .

energy [17]. However, it seems that $\tilde{E}_2 \sim 1.2$ and $2 \lesssim \tilde{E}'_2 < 3$ from Figs. 4 and 5. If $\tilde{E}'_2 - \tilde{E}_2 = 1$, the solution Φ_a^D for $a > -1/2$ is consistent with the TT solution in the same sense as the energy.

3.3 $|\Delta_S|$ and reality

Fig. 7 shows plots of $|\Delta_S|$ (2.21) for the “double brane” solution Φ_a^D at the truncation level L . With increasing level, it approaches zero for $a \geq -1/2$. This behavior is consistent with the equation of motion (2.4) for Φ_a^D . The extrapolation values are close to 0.25 for $a > -1/2$ except around $a = -1/2$, where they are unstable. We could expect that the above does not contradict that $|\Delta_S| \rightarrow 0$ ($L \rightarrow \infty$) for $a \geq -1/2$.

Figs. 8 and 9 show plots of Im/Re (2.22) for the “double brane” solution Φ_a^D at the truncation level L . With increasing level, it approaches zero for $a \geq -1/2$. This behavior is consistent with the reality condition of the string field Φ_a^D . In particular, from Fig. 9, we have found that $\text{Im}/\text{Re} = 0$ for $-0.469 \leq a \leq -0.463$ at $L = 20$ and for $-0.483 \leq a \leq -0.446$ at $L = 22$ (although there is no solution at $a = -0.468$ in both cases as mentioned). The region of a at $L = 22$, where Φ_a^D is real, is larger than that at $L = 20$. We can expect that it becomes larger at higher truncation level because Φ_a^D at the level $L + 2$ is real once it becomes real at the level L from our method to construct the solutions. We note that the regions of a such that Φ_a^D is real correspond to those where the value of $\text{Re } E_0[\Phi_a^D]$ shows irregular behavior in Fig. 5.

In Fig. 8, the extrapolation values become negative for some region of a although Im/Re should be nonnegative by its definition (2.22). We might interpret that Φ_a^D becomes real at finite level in such a region.

From the above observations, we expect that the “double brane” solution Φ_a^D for $a \geq -1/2$ satisfies the reality condition in the large level limit $L \rightarrow \infty$.

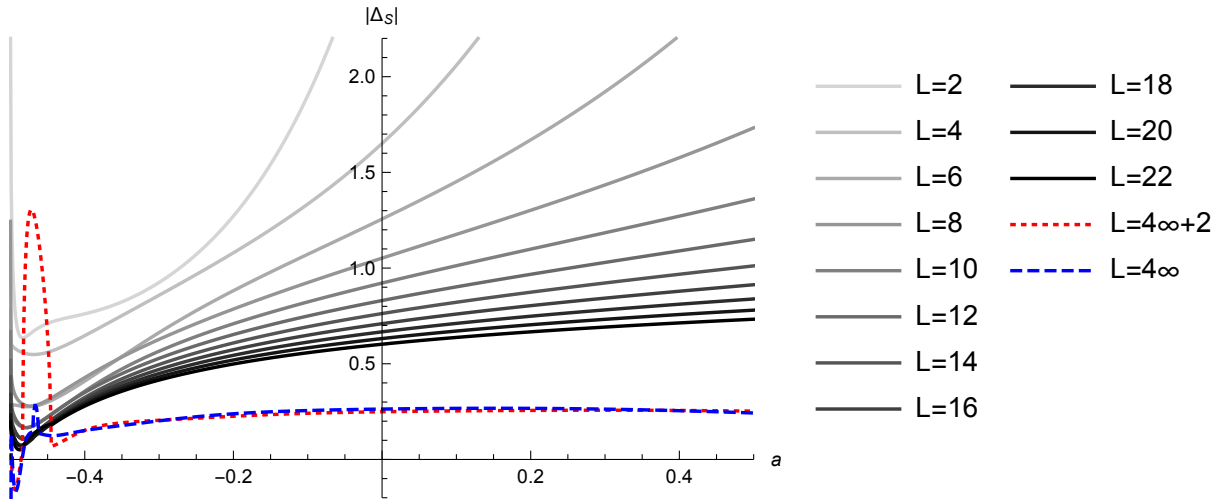


Figure 7: Plots of $|\Delta_S|$ (2.21) for the “double brane” solution Φ_a^D at the truncation level L . The horizontal axis denotes the value of the parameter a .

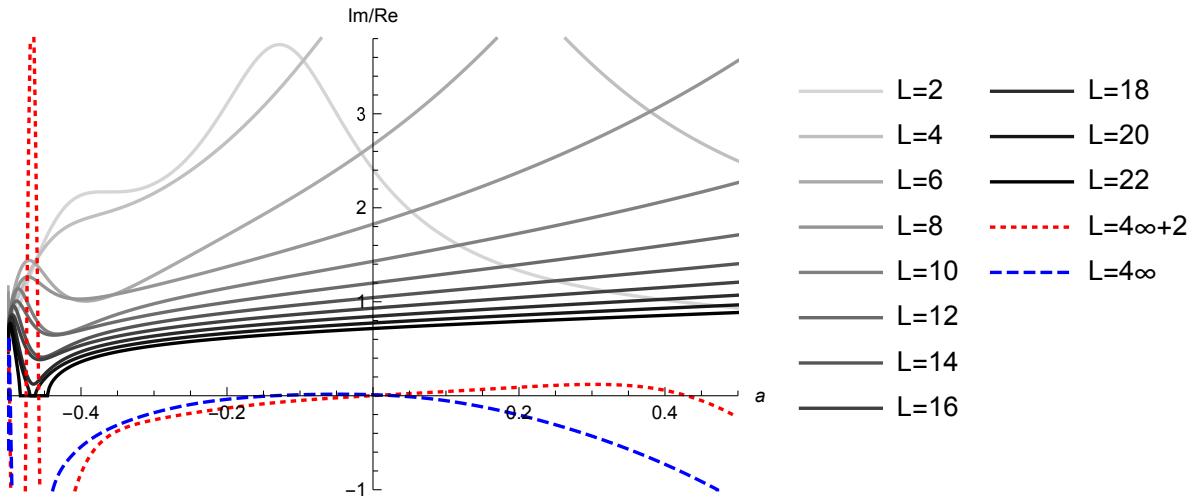


Figure 8: Plots of Im/Re (2.22) for the “double brane” solution Φ_a^D at the truncation level L . The horizontal axis denotes the value of the parameter a .

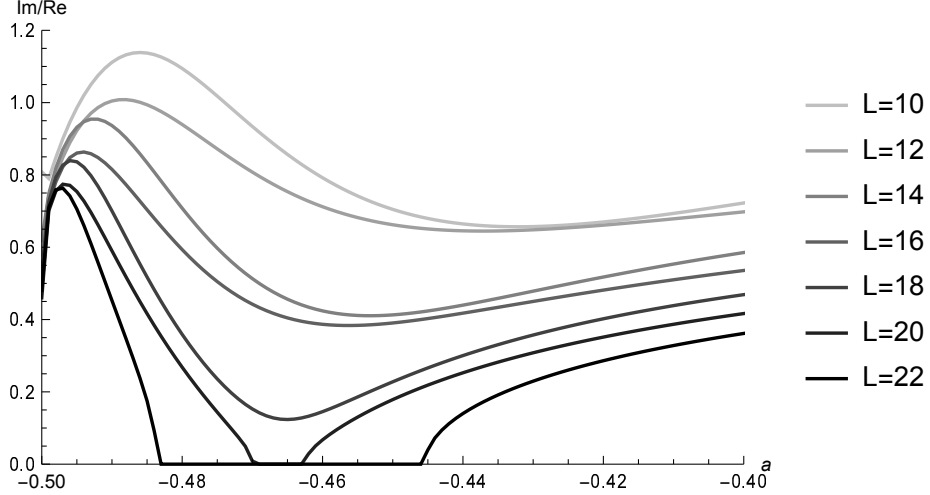


Figure 9: Plots of Im/Re (2.22) for the “double brane” solution Φ_a^D such as $a \gtrsim -1/2$ at the truncation level $L = 10, 12, \dots, 22$. The horizontal axis denotes the value of the parameter a . The vertical axis stands at $a = -1/2$.

4 “Ghost brane” solution

Our strategy to construct solutions corresponding to “ghost brane” is the same as that in §3.

In the theory around the perturbative vacuum, which is the case $a = 0$ in (2.1), a “ghost brane” solution $\Phi_{a=0}^G$ is obtained from one of complex solutions at the truncation level 4. Taking a solution $\Phi_{a=0}^G$ at level L as an initial string field, we can obtain $\Phi_{a=0}^G$ at level $L + 2$ by Newton’s method. Such a solution $\Phi_{a=0}^G$ coincides with the “ghost brane” solution in [5].

Firstly, at the truncation level 4, we constructed Φ_a^G ($-1/2 \leq a \leq 1/2$) from $\Phi_{a=0}^G$. Then, for a fixed value of a , which is one of $a = -0.5, -0.499, -0.498, \dots, 0.499, 0.5$, we constructed higher level solutions from Φ_a^G at level 4 up to 22. As a result, we have obtained numerical solutions Φ_a^G , except for $\Phi_{a=-0.499}^G$ at level 22. In the case $a = -0.499$, Newton’s method for constructing a solution at level 22 did not converge.

4.1 Energy

Figs. 10 and 11 show plots of the energy E (2.15) for the “ghost brane” solution Φ_a^G at the truncation level L . As in Fig. 10, the real part $\text{Re} E[\Phi_a^G]$ increases with increasing level. The extrapolations are close to -1 for $a > -1/2$. There is a maximum near $a = -1/2$ for each extrapolation and the maximum value is greater than zero.

As in Fig. 11, the imaginary part $\text{Im} E[\Phi_a^G]$ approaches zero with increasing level. In particular, extrapolation values are close to zero for $a > -1/2$ although they become unstable around $a = -1/2$. We note that $\text{Im} E[\Phi_a^G] = 0$ at $a = -1/2$ for the level $L \geq 6$ as in Table 2 in appendix A.

From the above, we might expect that the energy for the “ghost brane” solution behaves as

$$E[\Phi_a^G] \rightarrow \begin{cases} E_{-1} & (a > -1/2) \\ E'_{-1} & (a = -1/2) \end{cases} \quad (L \rightarrow \infty), \quad (4.1)$$

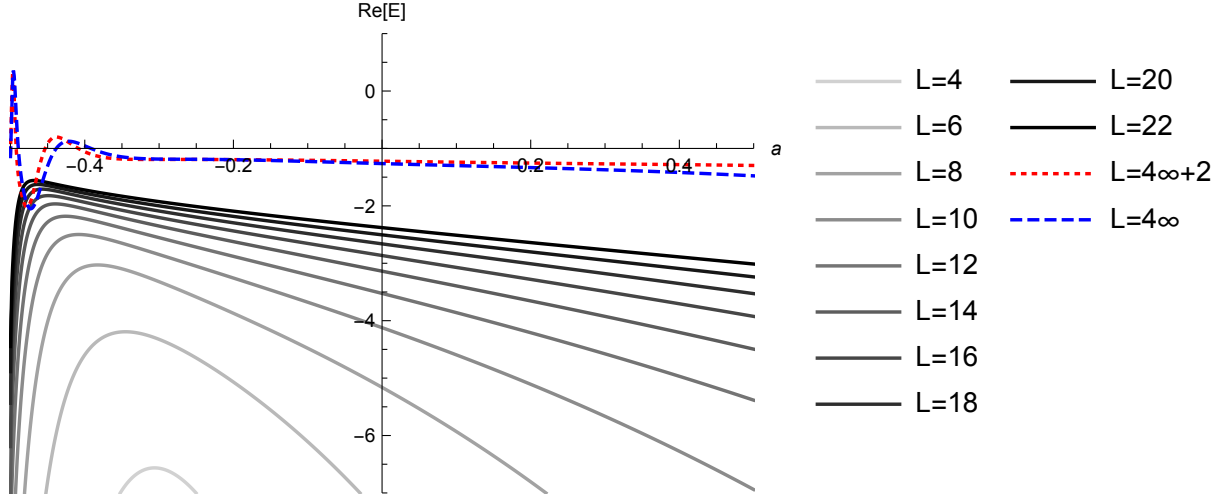


Figure 10: Plots of the real part of the energy E (2.15) for the “ghost brane” solution Φ_a^G at the truncation level L . The dotted and dashed lines are extrapolations to $L = 4k + 2$ ($k \rightarrow \infty$) and $L = 4k$ ($k \rightarrow \infty$), respectively. The horizontal axis denotes the value of the parameter a at $\text{Re } E = -1$.

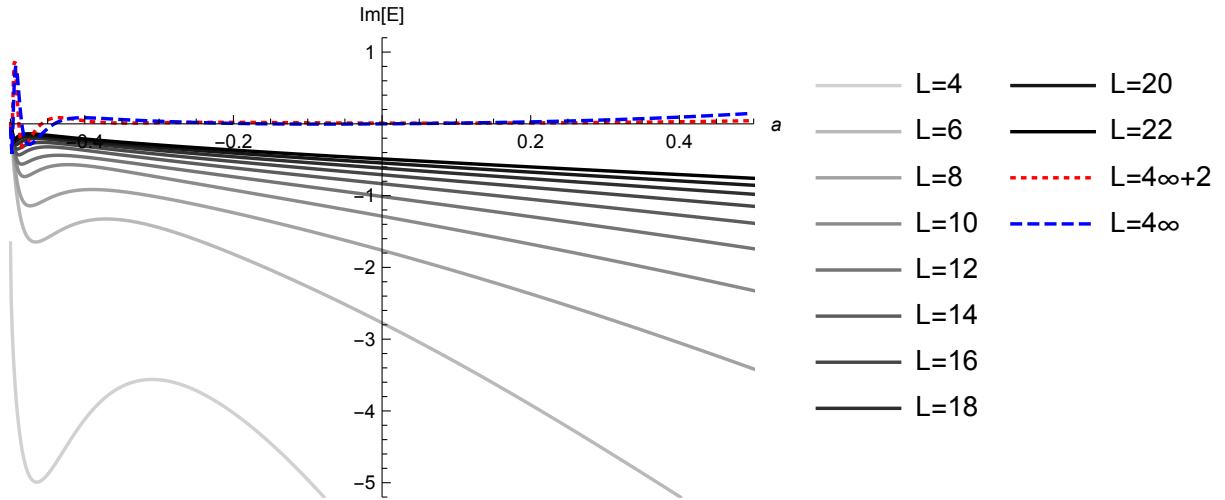


Figure 11: Plots of the imaginary part of the energy E (2.15) for the “ghost brane” solution Φ_a^G at the truncation level L . The dotted and dashed lines are extrapolations to $L = 4k + 2$ ($k \rightarrow \infty$) and $L = 4k$ ($k \rightarrow \infty$), respectively. The horizontal axis denotes the value of the parameter a .

where E_{-1} and E'_{-1} seem to be real constants such as $-2 < E_{-1} < E'_{-1}$, in a similar way to (3.1) for Φ_a^D , but it is more obscure in this case. If we focus on the extrapolation values, it seems that $E_{-1} \sim -1.25$ and $0 < E'_{-1} < 1$, although Φ_a^G could represent ghost brane literally if $E_{-1} = -1$ and $E'_{-1} = 0$. If $E'_{-1} - E_{-1} = 1$, Φ_a^G for $a \geq -1/2$ is consistent with the a -dependence of the TT solution.

4.2 Gauge invariant observable

Figs. 12, 13, and 14 show plots of the gauge invariant observable E_0 (2.17) for the “ghost brane” solution Φ_a^G at the truncation level L . As in Fig. 12, the real part $\text{Re} E_0[\Phi_a^G]$ approaches -1 for $a > -1/2$. As in Fig. 13, there is a maximum near $a = -1/2$ for each level L . We have found that the maximum values are greater than -1 for $L \geq 10$ although there is a large error in extrapolation values of $\text{Re} E_0[\Phi_a^G]$ near $a = -1/2$ in Fig. 12.⁷

As in Fig. 14, the imaginary part $\text{Im} E_0[\Phi_a^G]$ decreases with increasing level. Its extrapolation values are about 0.1 for $a > -1/2$ and they become unstable around $a = -1/2$. At $a = -1/2$, $\text{Im} E_0[\Phi_a^G] = 0$ for the level $L \geq 6$ as in Table 2 in appendix A.

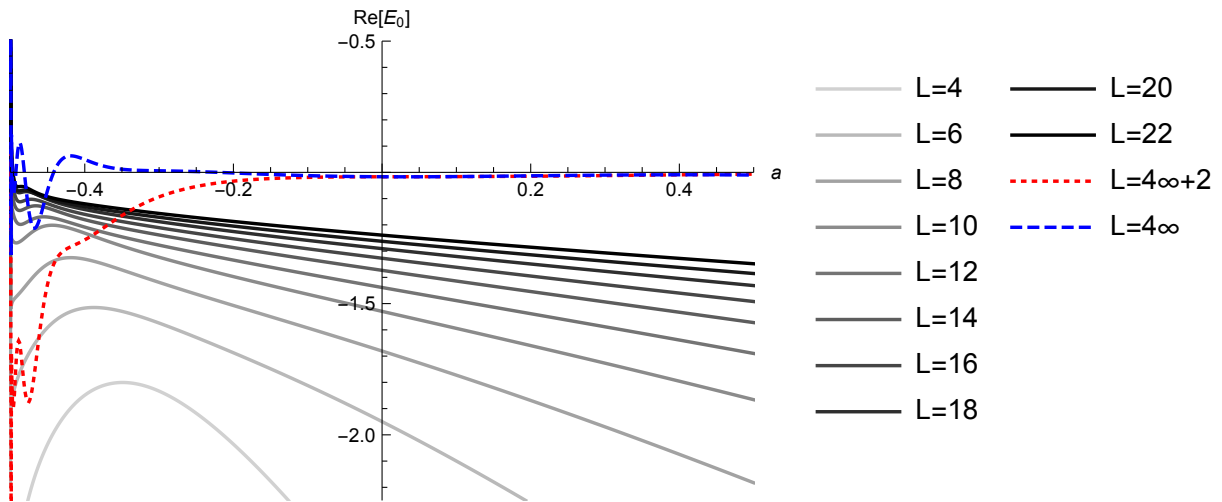


Figure 12: Plots of the real part of the gauge invariant observable E_0 (2.17) for the “ghost brane” solution Φ_a^G at the truncation level L . The dotted and dashed lines are extrapolations to $L = 4k + 2$ ($k \rightarrow \infty$) and $L = 4k$ ($k \rightarrow \infty$), respectively. The horizontal axis denotes the value of the parameter a at $\text{Re} E_0 = -1$.

From the above, in a similar way to (4.1), we could expect that the gauge invariant observable (2.17) behaves as

$$E_0[\Phi_a^G] \rightarrow \begin{cases} \tilde{E}_{-1} & (a > -1/2) \\ \tilde{E}'_{-1} & (a = -1/2) \end{cases} \quad (L \rightarrow \infty), \quad (4.2)$$

where \tilde{E}_{-1} and \tilde{E}'_{-1} seem to be real constants such as $-2 < \tilde{E}_{-1} < \tilde{E}'_{-1}$.

⁷We performed computations at $a = -0.5, -0.4999, -0.4998, \dots, -0.4901, -0.49$ in order to show details near $a = -0.5$ in Fig. 13 (and Fig. 12). In addition to $a = -0.499$ for $L = 22$, we did not obtain solutions at $a = -0.4989$ for $L = 20, 22$ and at $a = -0.4988$ for $L = 16, 18, 20, 22$.

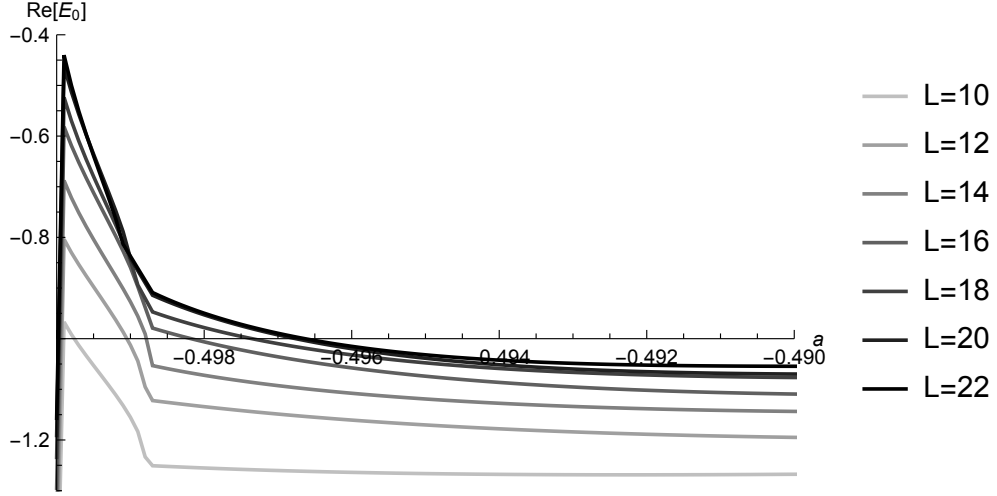


Figure 13: Plots of the real part of the gauge invariant observable E_0 (2.17) for the “ghost brane” solution Φ_a^G near $a = -1/2$ at the truncation level $L = 10, 12, \dots, 22$. The horizontal axis denotes the value of the parameter a at $\text{Re } E_0 = -1$. The vertical axis stands at $a = -1/2$.

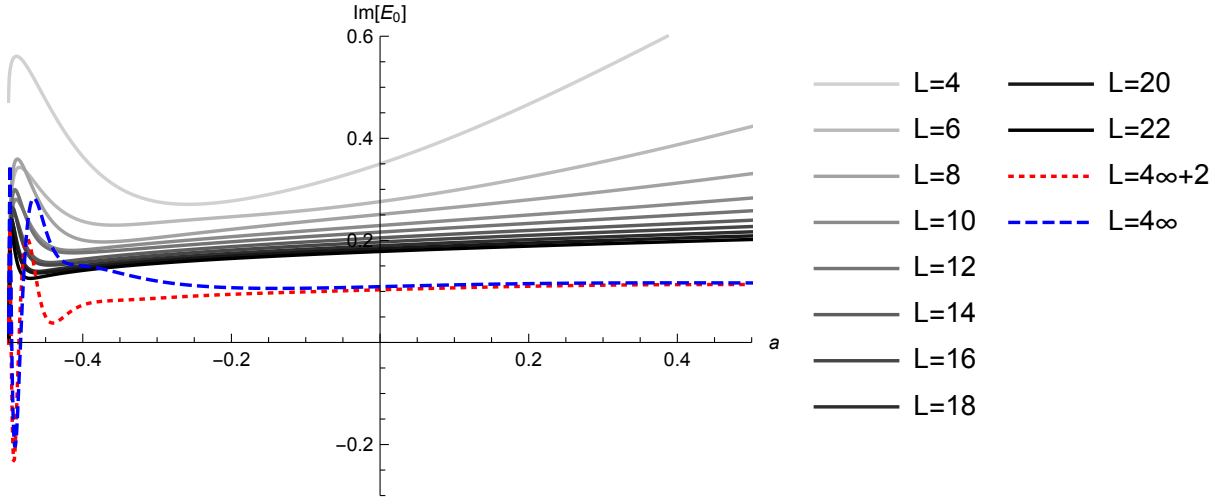


Figure 14: Plots of the imaginary part of the gauge invariant observable E_0 (2.17) for the “ghost brane” solution Φ_a^G at the truncation level L . The dotted and dashed lines are extrapolations to $L = 4k + 2$ ($k \rightarrow \infty$) and $L = 4k$ ($k \rightarrow \infty$), respectively. The horizontal axis denotes the value of the parameter a .

4.3 $|\Delta_S|$ and reality

Fig. 15 shows plots of $|\Delta_S|$ (2.21) for the “ghost brane” solution Φ_a^G at the truncation level L . It decreases with increasing level. The extrapolation values are about 0.1 for $a \gtrsim -1/2$ and they are close to zero near $a = -1/2$. It is consistent with the equation of motion (2.4) for Φ_a^G .

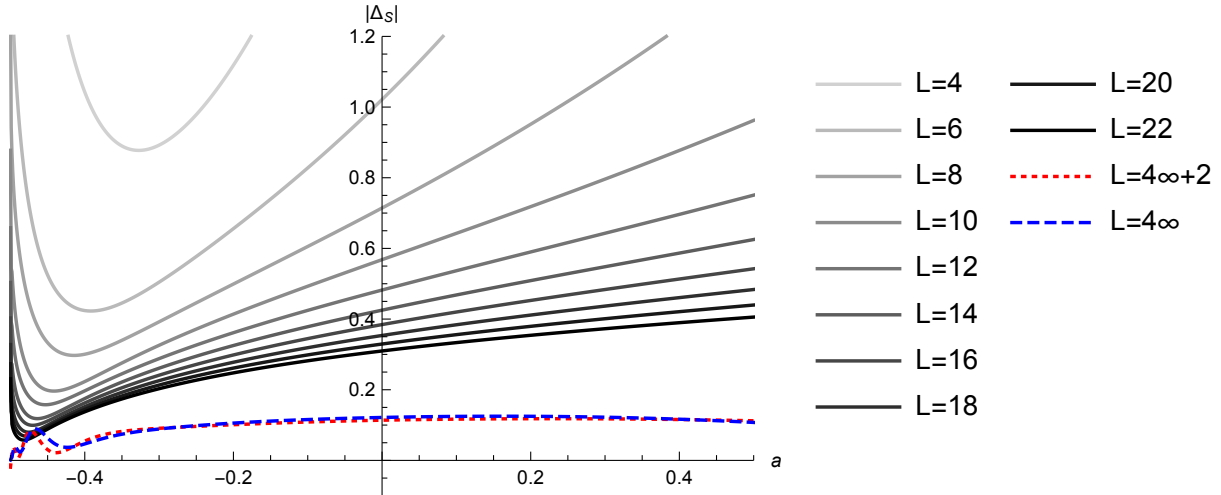


Figure 15: Plots of $|\Delta_S|$ (2.21) for the “ghost brane” solution Φ_a^G at the truncation level L . The horizontal axis denotes the value of the parameter a .

Fig. 16 shows plots of Im/Re (2.22) for the “ghost brane” solution Φ_a^G at the truncation level L . For $a \gtrsim -0.4$, Im/Re at level L up to 22 and its extrapolation values are greater than 0.2. On the other hand, we found that $\text{Im}/\text{Re}[\Phi_a^G] = 0$ at $a = -0.5, -0.499$ for $L \geq 6$, although there is no solution at $a = -0.499$ for $L = 22$.

In any case, it seems that Φ_a^G does not satisfy the reality condition for $a \gtrsim -0.4$ even at the limit $L \rightarrow \infty$ from the numerical behavior of $\text{Im}/\text{Re}[\Phi_a^G]$ in Fig. 16 and comparison with that for Φ_a^D in Fig. 8. It is consistent with the interpretation of the “ghost brane” solution in [5], which corresponds to the case $a = 0$.

5 Concluding remarks

In this paper, we have numerically constructed the “double brane” solution Φ_a^D and the “ghost brane” solution Φ_a^G in the theory around the TT solution with a real parameter a by using the level truncation method. In particular, in the case $a = 0$, they coincide with the “double brane” and “ghost brane” solutions found by Kudrna and Schnabl. In this sense, our solutions are generalization of theirs. We have evaluated the energy E and gauge invariant observable E_0 for the obtained solutions and calculated $|\Delta_S|$ and Im/Re as a consistency check.

From our results, in the large level limit, it seems that $E[\Phi_a^D] \rightarrow E_2$ for $a > -1/2$ and $\rightarrow E'_2$ for $a = -1/2$, where the real constants, E_2 and E'_2 , satisfy $1 < E_2 < E'_2$. If $E_2 = 2 = E'_2 - 1$, Φ_a^D could be interpreted as double brane solution for $a \geq -1/2$ literally, but we observed $E_2 \sim 1.5$ and $2 < E'_2 < 3$ from our numerical result. However, the solution Φ_a^D for $a \geq -1/2$ is consistent with the

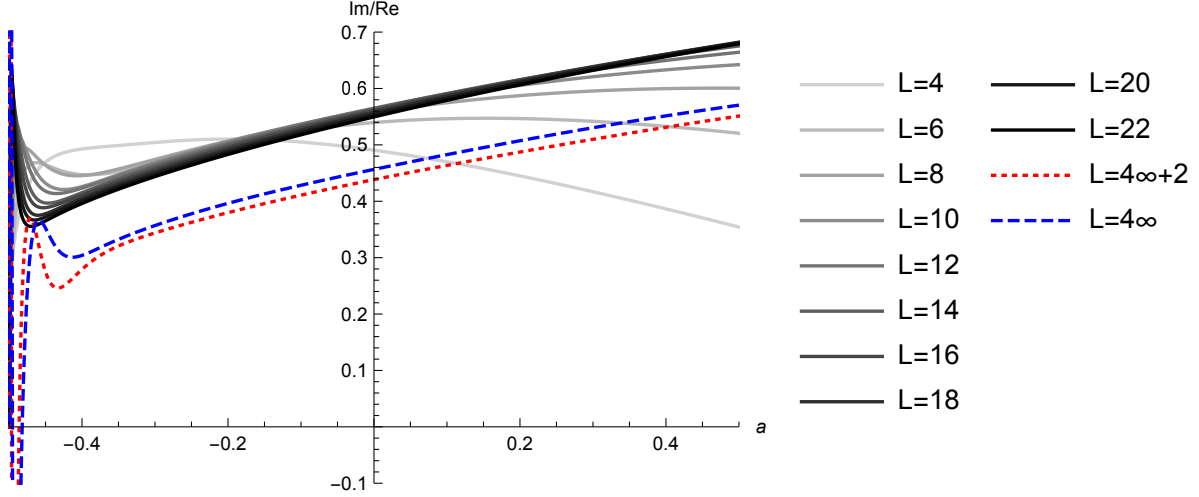


Figure 16: Plots of Im/Re (2.22) for the “ghost brane” solution Φ_a^G at the truncation level L . The horizontal axis denotes the value of the parameter a .

interpretation that the TT solution represents the tachyon vacuum at $a = -1/2$ and is pure gauge for $a > -1/2$ if $E'_2 - E_2 = 1$, which may hold. The value of $E_0[\Phi_a^D]$ behaves in a similar way to $E[\Phi_a^D]$ numerically. In order to establish the relation $E'_2 - E_2 = 1$, detailed computations around $a = -1/2$ for higher levels will be necessary. As for Φ_a^G , numerical behavior of the energy and gauge invariant observable is similar to that of Φ_a^D , but it is more ambiguous.

We observed that both $|\Delta_S[\Phi_a^D]|$ and $|\Delta_S[\Phi_a^G]|$ approach zero with increasing level, which is consistent with the projected equation of motion: $b_0 c_0(Q'\Phi + \Phi * \Phi) = 0$ up to the lowest level. We should check coefficients of higher level states in order to confirm the BRST invariance of solutions in Siegel gauge. It remains as a future work.

The numerical solutions Φ_a^D and Φ_a^G are constructed from complex solutions at level 2 and 4, respectively. Namely, they do not satisfy the reality condition of string field and therefore E and E_0 for them have imaginary part in general. However, we observed that $\text{Im}/\text{Re}[\Phi_a^D] \rightarrow 0$ with increasing level for $a \geq -1/2$. In particular, we found a region of a where $\text{Im}/\text{Re}[\Phi_a^D] = 0$ at the level 20 and 22. In this sense, Φ_a^D is expected to be real at the large level limit for $a \geq -1/2$. As for Φ_a^G , it seems that $\text{Im}/\text{Re}[\Phi_a^G]$ does not approach zero with increasing level for $a \gtrsim -0.4$, although we found that at $a = -0.5$ and $a = -0.499$, $\text{Im}/\text{Re}[\Phi_a^G] = 0$ for the level $L \geq 6$.

We have constructed numerical solutions by Newton’s method, where we have to choose appropriate initial configurations for the iterative algorithm. In this paper, we have adopted a choice explained in §3: 1. At the lowest truncation level, which is two for Φ_a^D and four for Φ_a^G , we have constructed solutions for various values of a from $\Phi_{a=0}^D$ and $\Phi_{a=0}^G$ by varying the value of a little by little. 2. For each value of a , higher level solutions have been constructed level by level. However, we can make another choice of initial configurations: 1’. For $a = 0$, we construct higher level solutions level by level. 2’. At each level, solutions for $a \neq 0$ are constructed from that for $a = 0$ by varying the value of a little by little. We have observed that there is a possibility of obtaining different solutions by 1’-2’ from those by 1-2, where solutions become real near $a = -1/2$. Further detailed investigation is a future problem although the procedure 1’-2’ takes more time for calculation.

In this paper, we have adopted a method of extrapolations, which is explained in §3.1. There are two extrapolation values: one is for the truncation level $L = 4\infty + 2$ and the other is for $L = 4\infty$, which are plotted in Figures by dotted and dashed lines. The difference of them would correspond to an error of the extrapolation. We should justify the extrapolation method or adopt other methods in order to refine the numerical results.

We have performed calculations in Siegel gauge for simplicity. It is desirable to evaluate gauge invariants in other gauges for “double brane” and “ghost brane” solutions to understand them further. We are preparing computations of them in Asano-Kato gauge [18] as in [19, 20].⁸

Acknowledgments

This work was supported in part by JSPS KAKENHI Grant Numbers JP20K03933, JP20K03972. The numerical calculations were partly carried out on sushiki and XC40 at YITP in Kyoto University.

A Some numerical data for solutions

A.1 Numerical data for solutions at $a = -1/2$

We list explicit numerical values of solutions in the theory around the TT solution at $a = -1/2$ in Tables 1 and 2. They can be compared with those in [5], which correspond to the case $a = 0$.⁹

The data in Table 1 are E (2.15), E_0 (2.17), $|\Delta_S|$ (2.21), and Im/Re (2.22) for the “double brane” solution $\Phi_{a=-1/2}^D$ and they correspond to points at $a = -1/2$ in Figs. 1, 2, 3, 4, 5, 6, 7, 8, and 9. The data in Table 2 are E (2.15), E_0 (2.17), $|\Delta_S|$ (2.21), and Im/Re (2.22) for the “ghost brane” solution $\Phi_{a=-1/2}^G$ and they correspond to points at $a = -1/2$ in Figs. 10, 11, 12, 13, 14, 15, and 16.

A.2 Coefficients of lowest level states for the solutions

We list numerical data of three component fields for the solutions, Φ_a^D and Φ_a^G , at $a = -1/2$ in Tables 3 and 4. They can be compared with those of the solutions at $a = 0$ listed in [5]. Furthermore, we plot the coefficient of the lowest level state $c_1|0\rangle$, or the tachyon field as a component, of Φ_a^D and Φ_a^G for $a \geq -1/2$ in Figs. 17, 18, 19, and 20. The data in the column of $c_1|0\rangle$ in Table 3 correspond to points at $a = -1/2$ in Figs. 17 and 18. The data in the column of $c_1|0\rangle$ in Table 4 correspond to points at $a = -1/2$ in Figs. 19 and 20.

Roughly, from Fig. 18, we can see that the imaginary part of the tachyon field of Φ_a^D vanishes with increasing level for $a \geq -1/2$. On the other hand, from Fig. 20, it seems that the imaginary part of the tachyon field of Φ_a^G remains nonzero with increasing level for $a \gtrsim -0.4$.

A.3 Evaluation of quadratic identities

It is known that solutions to the equation of motion in open string field theory satisfy certain quadratic identities [22]. Here, we show some numerical data for evaluation of them as a consistency check

⁸Some comments can be found on calculations in Schnabl gauge in [21].

⁹Our definition of Im/Re seems to be different from that in [5]. We suspect that a choice of a basis (or its normalization) is different.

Table 1: E (2.15), E_0 (2.17), $|\Delta_S|$ (2.21), and Im/Re (2.22) for the “double brane” solution $\Phi_{a=-1/2}^D$ at the truncation level L .

L	E	E_0	$ \Delta_S $	Im/Re
2	$-0.738519 + 6.42573i$	$2.5906 - 0.611421i$	2.27577	0.414127
4	$-0.520622 - 3.02656i$	$2.7175 - 0.100579i$	0.624772	0.664631
6	$-0.810759 - 1.90909i$	$2.62035 - 0.100411i$	0.781281	1.15795
8	$1.2739 - 1.27992i$	$2.59001 - 0.122603i$	1.24412	1.09292
10	$0.947834 - 1.30151i$	$2.38848 + 0.0741147i$	0.667769	0.80842
12	$1.55586 - 1.07501i$	$2.35887 + 0.0660807i$	0.517581	0.57895
14	$1.51726 - 0.904625i$	$2.2996 + 0.0707516i$	0.431135	0.617605
16	$1.78862 - 0.768909i$	$2.25904 + 0.0906131i$	0.339793	0.501388
18	$1.7433 - 0.660931i$	$2.22563 + 0.0962804i$	0.283798	0.531292
20	$1.89055 - 0.579279i$	$2.21258 + 0.0902456i$	0.232422	0.460356
22	$1.85117 - 0.508455i$	$2.19168 + 0.0854377i$	0.195764	0.481028

Table 2: E (2.15), E_0 (2.17), $|\Delta_S|$ (2.21), and Im/Re (2.22) for the “ghost brane” solution $\Phi_{a=-1/2}^G$ at the truncation level L . $\Phi_{a=-1/2}^G$ satisfies the reality condition for $L \geq 6$.

L	E	E_0	$ \Delta_S $	Im/Re
4	$-58.3862 - 1.66004i$	$-2.95681 + 0.472707i$	4.66418	0.189811
6	-24.413	-2.19698	1.91163	0
8	-15.6787	-1.81939	1.29319	0
10	-11.1078	-1.58933	0.87768	0
12	-8.76291	-1.46405	0.65827	0
14	-7.20365	-1.37387	0.503632	0
16	-6.19244	-1.29508	0.40301	0
18	-5.43759	-1.23428	0.327863	0
20	-4.88756	-1.19106	0.273432	0
22	-4.44884	-1.15705	0.230936	0

Table 3: Coefficients of three lowest level states for the “double brane” solution $\Phi_{a=-1/2}^D$ at the truncation level L .

L	$c_1 0\rangle$	$L_{-2}^{\text{mat}}c_1 0\rangle$	$L_{-2}^{\text{gh}'}c_1 0\rangle$
2	$-1.62421 - 0.556839i$	$-0.144175 - 0.362514i$	$0.179079 - 0.141459i$
4	$-0.811826 - 0.492565i$	$0.0805148 - 0.211769i$	$0.0936975 - 0.0673882i$
6	$-0.617433 - 0.708114i$	$0.169208 - 0.223221i$	$0.0939303 - 0.0907553i$
8	$-0.46957 - 0.539068i$	$0.190683 - 0.158602i$	$0.127765 - 0.0634097i$
10	$-0.594608 - 0.464836i$	$0.110538 - 0.147441i$	$0.0882257 - 0.0634936i$
12	$-0.603815 - 0.328377i$	$0.0657693 - 0.115888i$	$0.084529 - 0.0536261i$
14	$-0.614146 - 0.359062i$	$0.0612609 - 0.120976i$	$0.0742589 - 0.05115i$
16	$-0.598281 - 0.280436i$	$0.0377076 - 0.0991098i$	$0.0693785 - 0.0454664i$
18	$-0.611011 - 0.304459i$	$0.0339221 - 0.106696i$	$0.0626943 - 0.045099i$
20	$-0.589014 - 0.25289i$	$0.0208091 - 0.0900697i$	$0.058484 - 0.0407456i$
22	$-0.601353 - 0.269899i$	$0.0173314 - 0.0970247i$	$0.0539424 - 0.0413202i$

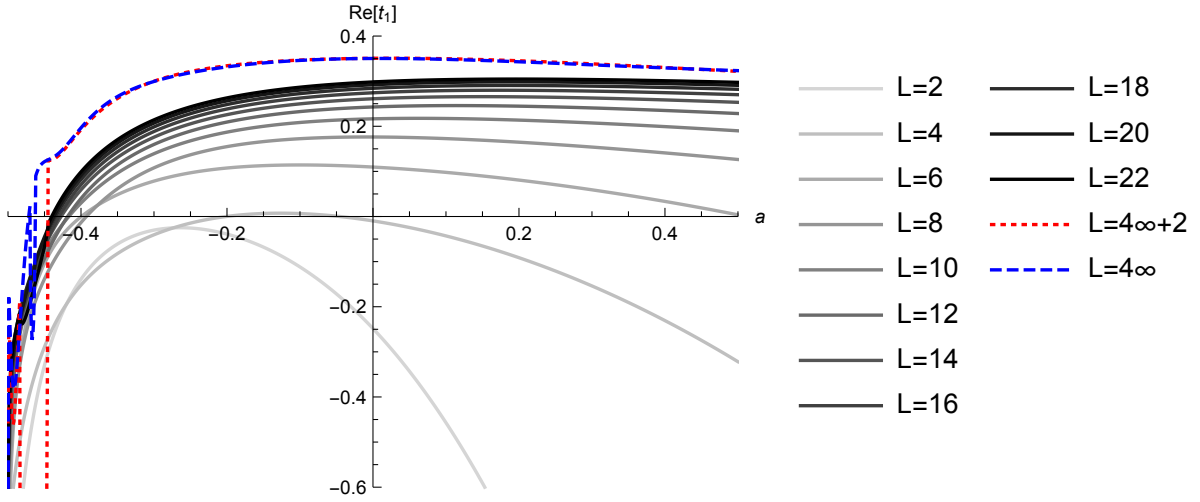


Figure 17: Plots of the real part of the coefficient of the lowest level state $c_1|0\rangle$ for the “double brane” solution Φ_a^D at the truncation level L . The dotted and dashed lines are extrapolations to $L = 4k + 2$ ($k \rightarrow \infty$) and $L = 4k$ ($k \rightarrow \infty$), respectively. The horizontal axis denotes the values of the parameter a .

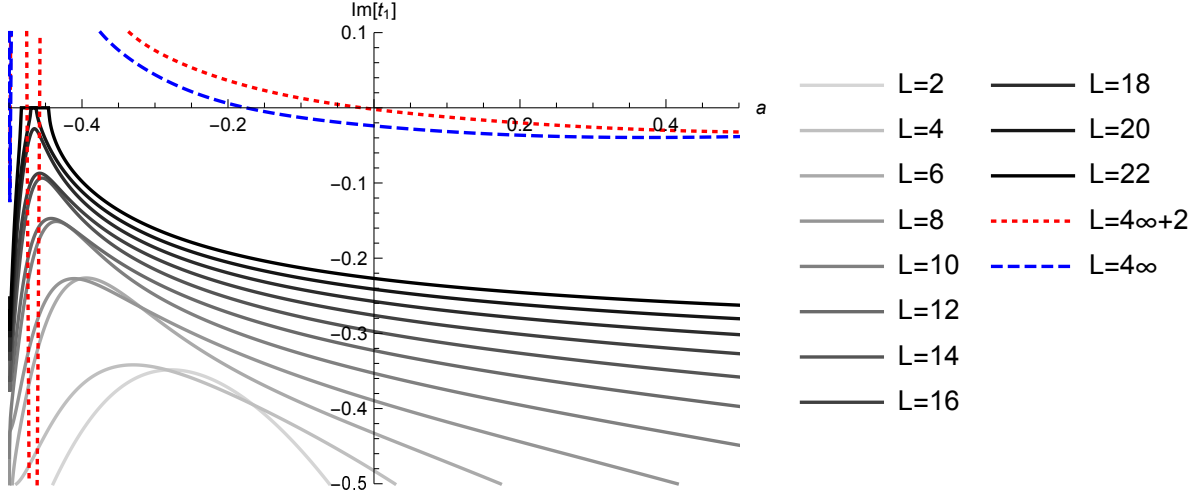


Figure 18: Plots of the imaginary part of the coefficient of the lowest level state $c_1|0\rangle$ for the “double brane” solution Φ_a^D at the truncation level L . The dotted and dashed lines are extrapolations to $L = 4k + 2$ ($k \rightarrow \infty$) and $L = 4k$ ($k \rightarrow \infty$), respectively. The horizontal axis denotes the values of the parameter a .

Table 4: Coefficients of three lowest level states for the “ghost brane” solution $\Phi_{a=-1/2}^G$ at the truncation level L .

L	$c_1 0\rangle$	$L_{-2}^{\text{mat}}c_1 0\rangle$	$L_{-2}^{\text{gh}'}c_1 0\rangle$
4	$-0.761439 - 0.415565i$	$-0.0430207 - 0.0388406i$	$1.44204 + 0.0481819i$
6	-0.360559	-0.0188028	0.675305
8	-0.238314	-0.0162807	0.440174
10	-0.152385	-0.0120697	0.310303
12	-0.11406	-0.0102722	0.234504
14	-0.0876269	-0.00885158	0.184856
16	-0.0708067	-0.00777904	0.150024
18	-0.0584666	-0.00695981	0.124815
20	-0.0494588	-0.00625865	0.105564
22	-0.0425024	-0.00570499	0.0907437

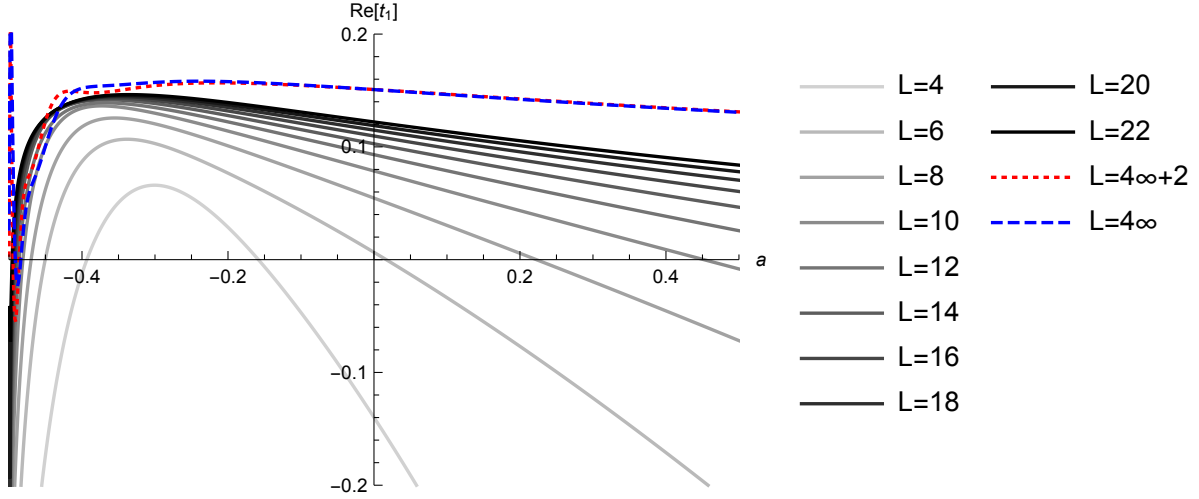


Figure 19: Plots of the real part of the coefficient of the lowest level state $c_1|0\rangle$ for the “ghost brane” solution Φ_a^G at the truncation level L . The dotted and dashed lines are extrapolations to $L = 4k + 2$ ($k \rightarrow \infty$) and $L = 4k$ ($k \rightarrow \infty$), respectively. The horizontal axis denotes the values of the parameter a .

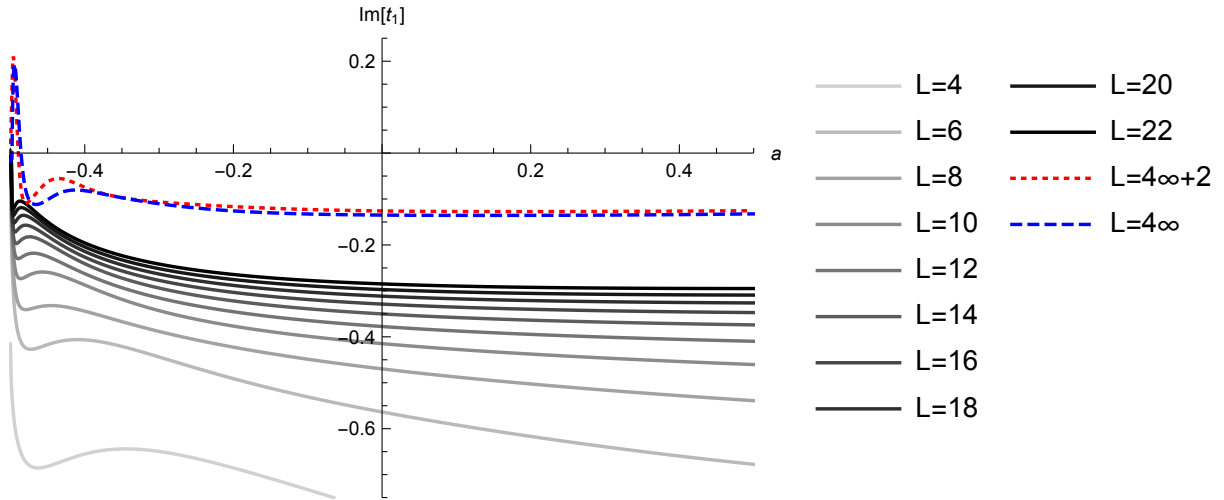


Figure 20: Plots of the imaginary part of the coefficient of the lowest level state $c_1|0\rangle$ for the “ghost brane” solution Φ_a^G at the truncation level L . The dotted and dashed lines are extrapolations to $L = 4k + 2$ ($k \rightarrow \infty$) and $L = 4k$ ($k \rightarrow \infty$), respectively. The horizontal axis denotes the values of the parameter a .

of numerical solutions in the theory around the TT solution with the parameter a . We can derive quadratic identities for solutions to (2.4):

$$\langle \Phi, [Q', L_n^{\text{mat}}] \Phi \rangle = -\frac{65}{54} (-1)^{\frac{n}{2}} n \delta_{n:\text{even}} \langle \Phi, Q' \Phi \rangle, \quad (\text{A.1})$$

$$\langle \Phi, [Q', L_n^{\text{tot}}] \Phi \rangle = -(-1)^{\frac{n}{2}} n \delta_{n:\text{even}} \langle \Phi, Q' \Phi \rangle, \quad (\text{A.2})$$

where $L_n^{\text{tot}} = L_n^{\text{mat}} + L_n^{\text{gh}}$, using symmetry of the interaction term of the action (2.1). Particularly, in the case of Siegel gauge solution Φ , if $\langle \Phi, c_0 L(a) \Phi \rangle \neq 0$, the ratios of the left hand side and the right hand side of the above equations with $n = 2m$:

$$R_m = \begin{cases} \frac{\langle \Phi, c_0 ((1+a)L_{2m}^{\text{mat}} + a\frac{m-1}{2m}L_{2m+2}^{\text{mat}} + a\frac{m+1}{2m}L_{2m-2}^{\text{mat}}) \Phi \rangle}{(-1)^m \frac{65}{54} \langle \Phi, c_0 ((1+a)(L_0^{\text{tot}} - 1) + aL_2^{\text{tot}} + 4aZ(a)) \Phi \rangle} & (m = 2, 3, 4, \dots) \\ \frac{-\langle \Phi, c_0 ((1+a)L_2^{\text{mat}} + aL_0^{\text{mat}} + \frac{13}{4}a) \Phi \rangle}{\frac{65}{54} \langle \Phi, c_0 ((1+a)(L_0^{\text{tot}} - 1) + aL_2^{\text{tot}} + 4aZ(a)) \Phi \rangle} & (m = 1) \end{cases}, \quad (\text{A.3})$$

$$\tilde{R}_m = \begin{cases} \frac{\langle \Phi, c_0 ((1+a)L_{2m}^{\text{tot}} + a\frac{m-1}{2m}L_{2m+2}^{\text{tot}} + a\frac{m+1}{2m}L_{2m-2}^{\text{tot}}) \Phi \rangle}{(-1)^m \langle \Phi, c_0 ((1+a)(L_0^{\text{tot}} - 1) + aL_2^{\text{tot}} + 4aZ(a)) \Phi \rangle} & (m = 2, 3, 4, \dots) \\ \frac{-\langle \Phi, c_0 ((1+a)L_2^{\text{tot}} + a(L_0^{\text{tot}} + 3)) \Phi \rangle}{\langle \Phi, c_0 ((1+a)(L_0^{\text{tot}} - 1) + aL_2^{\text{tot}} + 4aZ(a)) \Phi \rangle} & (m = 1) \end{cases} \quad (\text{A.4})$$

should be one identically¹⁰. We note that \tilde{R}_1 is one at $a = -1/2$ trivially.

We list some numerical data for the evaluations of R_m (A.3) and \tilde{R}_m (A.4) of the ‘‘double brane’’ solution at $a = -1/2$ in Tables 5 and 6 and those of the ‘‘ghost brane’’ solution at $a = -1/2$ in Tables 7 and 8. We also plot the value of R_1 of Φ_a^{D} in Figs. 21 and 22 and that of Φ_a^{G} in Figs. 23 and 24. Roughly, from these Figures, it seems that R_1 for Φ_a^{D} and Φ_a^{G} approaches one with increasing level although it is unstable around $a = -1/2$.

The above numerical behavior is consistent with quadratic identities $R_m = 1$ and $\tilde{R}_m = 1$ for solutions at $L = \infty$.

Table 5: R_m (A.3) of $\Phi_{a=-1/2}^{\text{D}}$ at the truncation level L for $m = 1, 2, 3, 4$.

L	R_1	R_2	R_3	R_4
2	0.911488 - 0.152245 <i>i</i>	-1.27584 + 0.412182 <i>i</i>	0	0
4	0.885585 + 0.021908 <i>i</i>	-1.28084 - 0.320084 <i>i</i>	-1.2104 - 0.84751 <i>i</i>	0
6	0.8729 + 0.0201808 <i>i</i>	-1.60019 + 1.10353 <i>i</i>	-1.59739 + 1.49291 <i>i</i>	-0.961762 + 0.978238 <i>i</i>
8	0.950585 + 0.00241884 <i>i</i>	2.06239 + 0.84862 <i>i</i>	3.66403 - 2.82962 <i>i</i>	-2.57524 - 3.66336 <i>i</i>
10	0.893514 + 0.0530564 <i>i</i>	-0.248418 + 1.30193 <i>i</i>	0.9719 + 1.85136 <i>i</i>	-1.11547 + 2.07613 <i>i</i>
12	0.937224 + 0.0359425 <i>i</i>	0.461938 + 0.777509 <i>i</i>	1.56888 + 0.298369 <i>i</i>	-0.28761 + 0.782399 <i>i</i>
14	0.929671 + 0.058921 <i>i</i>	0.597104 + 0.95585 <i>i</i>	1.36524 + 0.815189 <i>i</i>	-0.0304565 + 1.67951 <i>i</i>
16	0.953995 + 0.036186 <i>i</i>	0.765202 + 0.59013 <i>i</i>	1.27848 + 0.184195 <i>i</i>	0.324349 + 0.7959 <i>i</i>
18	0.953387 + 0.0515589 <i>i</i>	0.878275 + 0.620112 <i>i</i>	1.2123 + 0.34281 <i>i</i>	0.606532 + 1.09488 <i>i</i>
20	0.96477 + 0.0330054 <i>i</i>	0.890854 + 0.427151 <i>i</i>	1.12715 + 0.112292 <i>i</i>	0.678698 + 0.623308 <i>i</i>
22	0.966273 + 0.0431989 <i>i</i>	0.959863 + 0.420163 <i>i</i>	1.10173 + 0.175657 <i>i</i>	0.858197 + 0.707533 <i>i</i>

¹⁰The details can be found in [23], where numerical data for the tachyon vacuum and single brane solutions at $a = -1/2$, based on the solutions in [4], are listed up to level 26.

Table 6: \tilde{R}_m (A.4) of $\Phi_{a=-1/2}^D$ at the truncation level L for $m = 1, 2, 3, 4$.

L	\tilde{R}_1	\tilde{R}_2	\tilde{R}_3	\tilde{R}_4
2	1	$-1.49458 + 0.555977i$	0	0
4	1	$-1.3959 - 0.372793i$	$-1.32557 - 0.977179i$	0
6	1	$-1.82477 + 1.15122i$	$-1.89735 + 1.67941i$	$-1.1746 + 1.14418i$
8	1	$2.26372 + 0.934943i$	$4.01471 - 3.30933i$	$-2.90247 - 4.17631i$
10	1	$-0.344922 + 1.40266i$	$1.06346 + 2.07209i$	$-1.32026 + 2.17119i$
12	1	$0.467894 + 0.820665i$	$1.71676 + 0.257096i$	$-0.355223 + 0.778747i$
14	1	$0.596248 + 1.02744i$	$1.5074 + 0.860021i$	$-0.143872 + 1.76552i$
16	1	$0.786884 + 0.614174i$	$1.36667 + 0.142577i$	$0.294999 + 0.813055i$
18	1	$0.901552 + 0.656254i$	$1.30334 + 0.320084i$	$0.573704 + 1.15352i$
20	1	$0.914962 + 0.437798i$	$1.18301 + 0.0740143i$	$0.676277 + 0.637951i$
22	1	$0.9852 + 0.436868i$	$1.15838 + 0.139992i$	$0.859524 + 0.740684i$

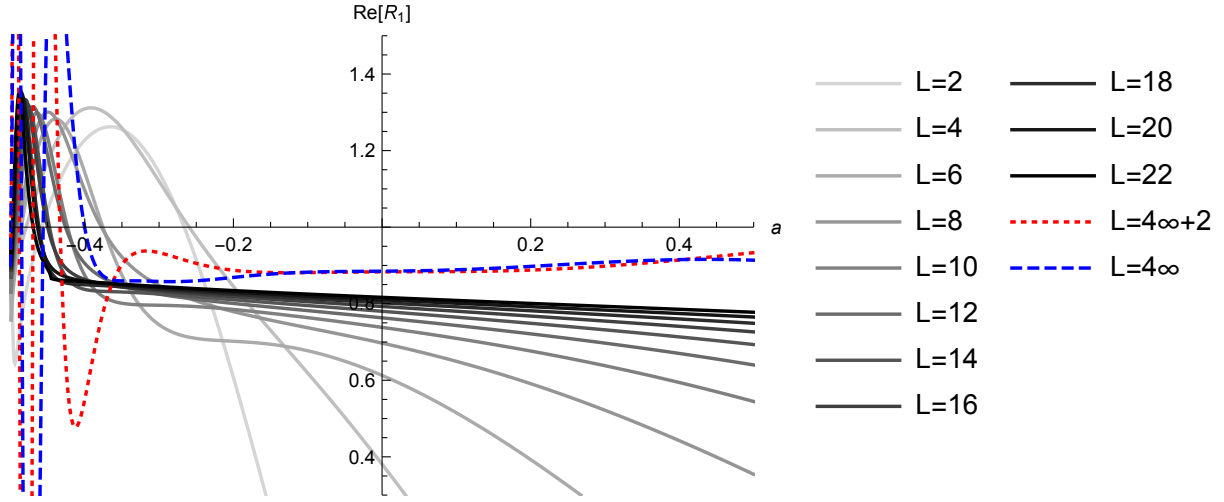


Figure 21: Plots of the real part of R_1 (A.3) of Φ_a^D at the truncation level L . The dotted and dashed lines are extrapolations to $L = 4k + 2$ and $L = 4k$ ($k \rightarrow \infty$), respectively. The horizontal axis denotes the value of the parameter a at $\text{Re } R_1 = 1$.

Table 7: R_m (A.3) of $\Phi_{a=-1/2}^G$ at the truncation level L for $m = 1, 2, 3, 4$.

L	R_1	R_2	R_3	R_4
4	$0.473669 - 0.0224943i$	$0.0290573 - 0.0136117i$	$-0.00391726 - 0.0214949i$	0
6	0.574357	0.142781	0.0199572	-0.00288513
8	0.6554	0.340813	0.152805	0.0118893
10	0.698864	0.479036	0.328676	0.100043
12	0.736879	0.566131	0.462773	0.244439
14	0.761953	0.631667	0.555784	0.373664
16	0.78442	0.677713	0.625193	0.473761
18	0.800922	0.714594	0.674924	0.551411
20	0.815886	0.742564	0.714176	0.610725
22	0.827609	0.765937	0.743846	0.657547

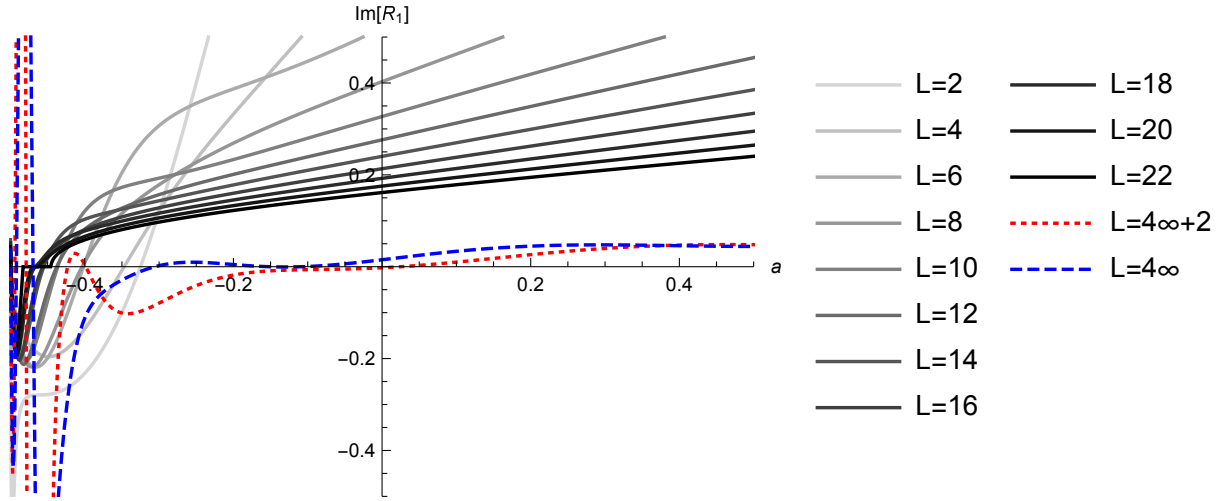


Figure 22: Plots of the imaginary part of R_1 (A.3) of Φ_a^D at the truncation level L . The dotted and dashed lines are extrapolations to $L = 4k + 2$ ($k \rightarrow \infty$) and $L = 4k$ ($k \rightarrow \infty$), respectively. The horizontal axis denotes the value of the parameter a .

Table 8: \tilde{R}_m (A.4) of $\Phi_{a=-1/2}^G$ at the truncation level L for $m = 1, 2, 3, 4$.

L	\tilde{R}_1	\tilde{R}_2	\tilde{R}_3	\tilde{R}_4
4	1	$-0.0219749 + 0.000400093i$	$-0.000350886 - 0.0220953i$	0
6	1	-0.0293363	0.029805	0.00101128
8	1	0.16492	0.215592	0.00493668
10	1	0.316654	0.431604	0.0656148
12	1	0.411717	0.583257	0.197593
14	1	0.490697	0.68693	0.318767
16	1	0.545656	0.758987	0.413544
18	1	0.592945	0.809749	0.489035
20	1	0.62858	0.847047	0.546827
22	1	0.659964	0.874591	0.593859

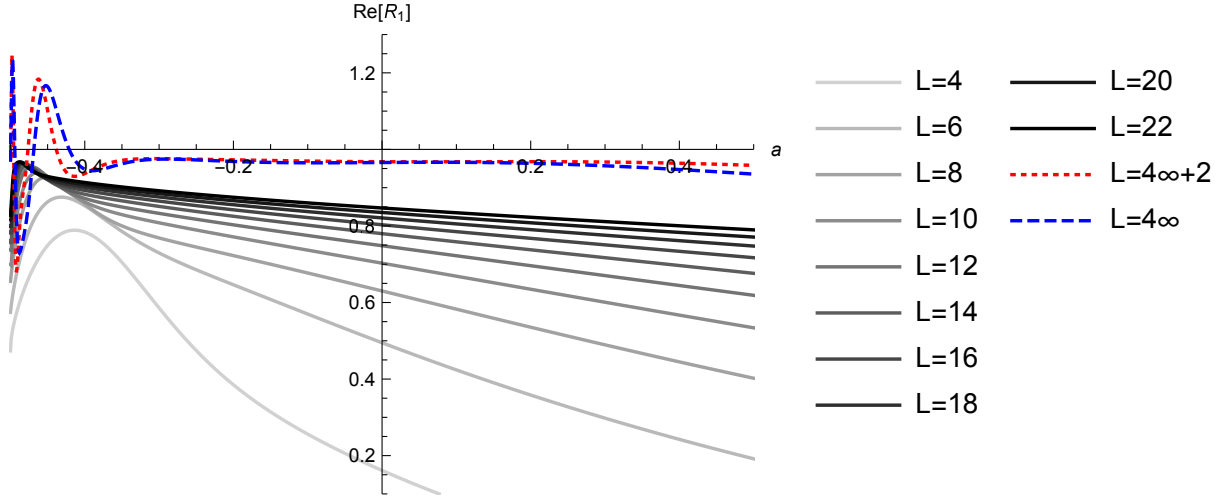


Figure 23: Plots of the real part of R_1 (A.3) of Φ_a^G at the truncation level L . The dotted and dashed lines are extrapolations to $L = 4k + 2$ ($k \rightarrow \infty$) and $L = 4k$ ($k \rightarrow \infty$), respectively. The horizontal axis denotes the value of the parameter a at $\text{Re} R_1 = 1$.

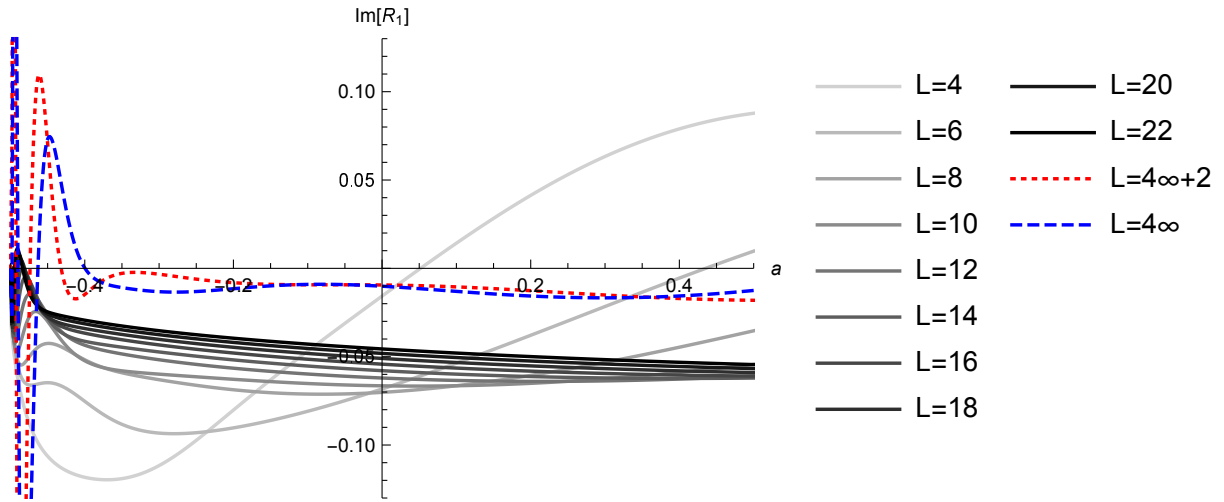


Figure 24: Plots of the imaginary part of R_1 (A.3) of Φ_a^G at the truncation level L . The dotted and dashed lines are extrapolations to $L = 4k + 2$ ($k \rightarrow \infty$) and $L = 4k$ ($k \rightarrow \infty$), respectively. The horizontal axis denotes the value of the parameter a .

References

- [1] A. Sen and B. Zwiebach, “Tachyon condensation in string field theory,” *JHEP* **03** (2000) 002, [arXiv:hep-th/9912249](#).
- [2] N. Moeller and W. Taylor, “Level truncation and the tachyon in open bosonic string field theory,” *Nucl. Phys. B* **583** (2000) 105–144, [arXiv:hep-th/0002237](#).
- [3] D. Gaiotto and L. Rastelli, “Experimental string field theory,” *JHEP* **08** (2003) 048, [arXiv:hep-th/0211012](#).
- [4] I. Kishimoto, “On numerical solutions in open string field theory,” *Prog. Theor. Phys. Suppl.* **188** (2011) 155–162.
- [5] M. Kudrna and M. Schnabl, “Universal Solutions in Open String Field Theory,” [arXiv:1812.03221 \[hep-th\]](#).
- [6] T. Takahashi and S. Tanimoto, “Marginal and scalar solutions in cubic open string field theory,” *JHEP* **03** (2002) 033, [arXiv:hep-th/0202133](#).
- [7] I. Kishimoto and T. Takahashi, “Open string field theory around universal solutions,” *Prog. Theor. Phys.* **108** (2002) 591–602, [arXiv:hep-th/0205275](#).
- [8] T. Takahashi, “Tachyon condensation and universal solutions in string field theory,” *Nucl. Phys. B* **670** (2003) 161–182, [arXiv:hep-th/0302182](#).
- [9] I. Kishimoto and T. Takahashi, “Vacuum structure around identity based solutions,” *Prog. Theor. Phys.* **122** (2009) 385–399, [arXiv:0904.1095 \[hep-th\]](#).
- [10] I. Kishimoto and T. Takahashi, “Exploring Vacuum Structure around Identity-Based Solutions,” *Theor. Math. Phys.* **163** (2010) 717–724, [arXiv:0910.3026 \[hep-th\]](#).
- [11] N. Ishibashi, “Comments on Takahashi-Tanimoto’s scalar solution,” *JHEP* **02** (2015) 168, [arXiv:1408.6319 \[hep-th\]](#).
- [12] I. Kishimoto, T. Masuda, and T. Takahashi, “Observables for identity-based tachyon vacuum solutions,” *PTEP* **2014** (2014) no. 10, 103B02, [arXiv:1408.6318 \[hep-th\]](#).
- [13] T. Kawano, I. Kishimoto, and T. Takahashi, “Gauge Invariant Overlaps for Classical Solutions in Open String Field Theory,” *Nucl. Phys. B* **803** (2008) 135–165, [arXiv:0804.1541 \[hep-th\]](#).
- [14] I. Ellwood, “The Closed string tadpole in open string field theory,” *JHEP* **08** (2008) 063, [arXiv:0804.1131 \[hep-th\]](#).
- [15] M. Schnabl, “Analytic solution for tachyon condensation in open string field theory,” *Adv. Theor. Math. Phys.* **10** (2006) no. 4, 433–501, [arXiv:hep-th/0511286](#).
- [16] H. Hata and S. Shinohara, “BRST invariance of the nonperturbative vacuum in bosonic open string field theory,” *JHEP* **09** (2000) 035, [arXiv:hep-th/0009105](#).

- [17] T. Baba and N. Ishibashi, “Energy from the gauge invariant observables,” *JHEP* **04** (2013) 050, [arXiv:1208.6206 \[hep-th\]](#).
- [18] M. Asano and M. Kato, “New Covariant Gauges in String Field Theory,” *Prog. Theor. Phys.* **117** (2007) 569–587, [arXiv:hep-th/0611189](#).
- [19] I. Kishimoto and T. Takahashi, “Numerical Evaluation of Gauge Invariants for a -gauge Solutions in Open String Field Theory,” *Prog. Theor. Phys.* **121** (2009) 695–710, [arXiv:0902.0445 \[hep-th\]](#).
- [20] I. Kishimoto and T. Takahashi, “Numerical Evaluation of Gauge Invariants for a -gauge Solutions in Open String Field Theory,” *Theor. Math. Phys.* **163** (2010) 710–716, [arXiv:0910.3025 \[hep-th\]](#).
- [21] E. Aldo Arroyo and M. Kudrna, “Numerical solution for tachyon vacuum in the Schnabl gauge,” *JHEP* **02** (2020) 065, [arXiv:1908.05330 \[hep-th\]](#).
- [22] M. Schnabl, “Constraints on the tachyon condensate from anomalous symmetries,” *Phys. Lett. B* **504** (2001) 61–63, [arXiv:hep-th/0011238](#).
- [23] I. Kishimoto, “Numerical evaluation of quadratic identities for classical solutions in open string field theory (in Japanese),” *Studies in Liberal Arts and Sciences, Tokyo University of Science* **53** (2021) (to be published).